THE JOURNAL OF BIOLOGICAL CHEMISTRY VOL. 287, NO. 2, pp. 1345–1360, January 6, 2012

Functional Analysis of DNA Replication Fork Reversal Catalyzed by *Mycobacterium tuberculosis* RuvAB Proteins*[S]

Received for publication, September 15, 2011, and in revised form, November 14, 2011 Published, JBC Papers in Press, November 17, 2011, DOI 10.1074/jbc.M111.304741

Jasbeer Singh Khanduja and K. Muniyappa[1]

From the Department of Biochemistry, Indian Institute of Science, Bangalore 560012, India

Background: Impediments to replication fork progression are an important source of genome instability and cell death.
Results: We reveal the functional characteristics of MtRuvAB complex.
Conclusion: MtRuvAB-catalyzed RFR is independent of symmetry at the fork junction, supercoiling and unimpeded by heterology.
Significance: An understanding of MtRuvAB complex functions, whose expression is up-regulated following infection, has implications for drug discovery and development.

Initially discovered in *Escherichia coli*, RuvAB proteins are ubiquitous in bacteria and play a dual role as molecular motor proteins responsible for branch migration of the Holliday junction(s) and reversal of stalled replication forks. Despite mounting genetic evidence for a crucial role of RuvA and RuvB proteins in reversal of stalled replication forks, the mechanistic aspects of this process are still not fully understood. Here, we elucidate the ability of *Mycobacterium tuberculosis* RuvAB (MtRuvAB) complex to catalyze the reversal of replication forks using a range of DNA replication fork substrates. Our studies show that MtRuvAB, unlike *E. coli* RuvAB, is able to drive replication fork reversal via the formation of Holliday junction intermediates, suggesting that RuvAB-catalyzed fork reversal involves concerted unwinding and annealing of nascent leading and lagging strands. We also demonstrate the reversal of replication forks carrying hemi-replicated DNA, indicating that MtRuvAB complex-catalyzed fork reversal is independent of symmetry at the fork junction. The fork reversal reaction catalyzed by MtRuvAB is coupled to ATP hydrolysis, is processive, and culminates in the formation of an extended reverse DNA arm. Notably, we found that sequence heterology failed to impede the fork reversal activity of MtRuvAB. We discuss the implications of these results in the context of recognition and processing of varied types of replication fork structures by RuvAB proteins.

The impediments to the progression of DNA replication fork have been shown to be one of the underlying causes of elevated levels of recombination, genome instability, and cell death in all organisms (1–5). Several lines of evidence suggest that DNA replication forks stall frequently due to the presence of DNA lesions, DNA secondary structures, DNA-protein complexes, transient depletion of the nucleotide pool, or due to the absence or impairment of essential replication proteins (1–6). Accumulating experimental evidence points out that cells possess a wide repertoire of proteins, including those of the homologous recombination (HR)[2] machinery, to remove blocks to fork progression and facilitate replication restart (2, 3, 7).

Studies on *Escherichia coli* and eukaryotic organisms suggest the recovery from replication arrest to be facilitated by recombination-dependent and/or -independent pathways, thus pointing toward the existence of many different types of substrates and the involvement of various proteins (2, 3, 7–10). In *E. coli*, PriA-dependent pathway is the major replication restart mechanism (11–13). PriA binds preferentially to the fork structures, D-loops, and replication intermediates and helps in the assembly of the functional replisome (12, 14). Studies of *E. coli* replication mutants have suggested a crucial role for HR components in the restoration of stalled replication forks through replication fork reversal (RFR) (8, 9, 15–17). A central feature of the RFR model posits unwinding of blocked forks with concomitant annealing of the nascent leading and lagging strand to form a four-stranded (chicken foot) intermediate resembling the HJ (17). In the presence of functionally active RecBCD and RecA, the HJs made as a result of fork reversal are processed by the RuvABC complex, thus leading to the generation of a fork structure suitable for PriA-mediated replication restart (8, 9, 12, 17). Cleavage of the HJ intermediate will result in the formation of one intact duplex and a second duplex with dsDNA end. HR between dsDNA end and the intact sister duplex will result in the formation of the D-loop that can be integrated into the PriA-mediated replication restart pathway (1–4).

In *E. coli*, resetting of the reversed replication forks by HR machinery can take place by several distinct mechanisms (2, 7–9). However, protein components or the mechanisms that govern reversal of the stalled forks and the formation of HJ

* This work was supported by European Community Grant CSI_LTB LSHP-CT-2007-037235, the Department of Biotechnology, New Delhi, under the "Centre of Excellence" in research on mycobacteria, and a J. C. Bose National Fellowship (to K. M.).
[S] This article contains supplemental Tables S1–S4, Figs. S1–S8, "Materials and Methods," "Results and Discussion," and additional references.
[1] To whom correspondence should be addressed. Tel.: 91-80-2293-2235/2360-0278; Fax: 91-80-2360-0814/0683; E-mail: kmbc@biochem.iisc.ernet.in.

[2] The abbreviations used are: HR, homologous recombination; HJ, Holliday junction; JM, joint molecule; MMS, methyl methanesulfonate; MtRuvA, *M. tuberculosis* RuvA protein; MtRuvB, *M. tuberculosis* RuvB protein; ODN, oligonucleotide; RF, replication fork; RFR, replication fork reversal; ssDNA, single-stranded DNA; ATPγS, adenosine 5′-*O*-(thiotriphosphate).

intermediates are not fully understood. One of the pathways posit a role for RecA in fork reversal and the generation of HJ intermediates that are subsequently processed to allow PriA-mediated replication restart (16). In general, the RuvAB complex is known to drive the branch migration of HJs, whereas RuvC facilitates the resolution of junctions (18–24). Several lines of evidence strongly support the notion that RuvA can assemble as a tetramer (complex I) or as an octamer (complex II) on the HJ intermediate (23, 25, 26, 28–32). Complex formation between RuvA-HJ causes significant structural distortions in DNA (25, 26). A recent study provided unequivocal evidence for the requirement of complex II in efficient HJ branch migration *in vitro* and RFR *in vivo* (33). *E. coli* RuvB protein is a hexameric DNA helicase that is recruited to the RuvA-Holliday junction complex, which in turn drives branch migration of the HJs (20, 27, 32, 34–36). Genetic evidence implicates the role of RuvAB complex not only in the processing of HJs generated by RFR but also as one of the initiator molecules for RFR. In *dnaEts*, *holD*^{Q10am}, and to some extent in *rep* helicase mutants, the RFR is catalyzed by RuvAB (15). In particular, isolation of *ruvA* and *ruvB* mutants impaired specifically for RFR underscores the fact that the RuvAB complex indeed plays a key role in the conversion of stalled forks into HJ intermediates (37, 38). Although genetic studies reveal that RuvAB complex can convert replication forks into an HJ, the biochemical and mechanistic aspects of this process remain to be elucidated.

Genetic and biochemical evidence suggests a role for RecG helicase in regression of stalled replication forks (39–41). Although a role for RecG in the processing of replication forks arrested by UV-induced damage was proposed, it has since been shown that in UV-irradiated *recG* or *ruvA ruvB* mutant cells, the arrested replication forks were maintained intact, and DNA synthesis resumed with kinetics that were similar to those in wild-type cells (42). In contrast, *E. coli* mutants with defects in both *ruvABC* and *recG* display extremely poor growth phenotypes, even in the absence of DNA damage, indicating their requirement during exponential cell growth (43). Despite the recent advances in our understanding of the expanding roles of RecG in processing of stalled replication forks, delineating its precise role is compounded by the lack of direct *in vivo* evidence supporting its role in fork reversal and by the fact that none of the pathways of RFR appear to require RecG (15, 43).

Although our understanding of the genetic basis of RFR catalyzed by *E. coli ruvA ruvB* is beginning to emerge, much less is known about the molecular mechanisms underlying RFR in mycobacteria and other organisms. Genome-wide transcriptome analyses of *Mycobacterium tuberculosis* from clinical lung tissues have shown up-regulation of *ruvA ruvB* expression (44), consistent with the notion that their gene products might be necessary for DNA replication/repair and to sustain a long term, persistent infection. We further note that two independent studies have clearly demonstrated the essentiality of *ruvA ruvB* genes for infection by *Borrelia burgdorferi*, the causative agent of Lyme disease (45, 46). To explore whether the *E. coli* paradigm can be generalized to other organisms, and to investigate the RFR activity of *M. tuberculosis* RuvAB complex, we used a series of synthetic substrates that mimic stalled replication fork intermediates. This approach is especially important because genetic analysis of *M. tuberculosis ruvA ruvB* and their role in the processing of stalled replication forks have not been elucidated. Our results reveal that *M. tuberculosis* RuvAB, unlike *E. coli* RuvAB (47), catalyzes the RFR reaction via the formation of Holliday junction. Furthermore, fork reversals catalyzed by MtRuvAB are independent of DNA supercoiling and are unimpeded by the presence of a short stretch of heterologous sequence.

EXPERIMENTAL PROCEDURES

Biochemicals, Plasmid DNA, Oligonucleotides, Bacterial Strains, and Enzymes—Fine chemicals were purchased from GE Healthcare and Sigma. Restriction endonucleases, T4 DNA ligase, T4 polynucleotide kinase, and *Pfu* polymerase were purchased from New England Biolabs, Ipswich, MA. Gene Ruler 50-bp DNA ladder (SM0371) and Gene Ruler ultra low range DNA ladder (SM01211) were procured from Fermentas Life Sciences. [γ-^{32}P]ATP was purchased from the Bhabha Atomic Research Center, Mumbai, India. Fast performance liquid chromatography columns were purchased from GE Healthcare. ODNs were purchased from Sigma Genosys. *E. coli* Rosetta2(DE3)pLysS strain and *pET 21a(+)* plasmid were purchased from Novagen, Madison, WI. *E. coli* HRS3401 is a Δ*ruvB*::*Km*^{R} derivative of *E. coli* AB1157. *E. coli* Rosetta2(DE3)pLysS (Δ*ruvB*::*Km*^{R}) strain was generated by moving the kanamycin resistance cassette from *E. coli* HRS3401 (Δ*ruvB*::*Km*^{R}), by P1 transduction, to *E. coli* Rosetta2(DE3)pLysS strain (48). *M. tuberculosis* RuvA was purified as described previously (26).

Construction of DNA Substrates—ODNs sequences are shown under supplemental Table 1. The ODNs were labeled at the 5′-end by using [γ-^{32}P]ATP, and fork substrates were generated in a two-step process by annealing the appropriate combinations of ODNs, as indicated under supplemental Table 2. For each substrate, we added stoichiometric amounts of purified ODNs to 100 μl of 0.3 M sodium citrate buffer (pH 7) containing 3 M NaCl. Reaction mixtures were heated for 5 min at 95 °C followed by slow cooling to 4 °C over a period of 2 h. Annealed substrates were gel-purified by electrophoresis on a 6% (w/v) polyacrylamide gel in 44.5 mM Tris borate buffer (pH 8.3) containing 0.5 mM EDTA. The bands corresponding to the individual substrates were excised from the gel and eluted into TE buffer (10 mM Tris-HCl (pH 7.5), 1 mM EDTA). The model replication fork substrates were prepared as described under supplemental "Materials and Methods".

Construction of M. tuberculosis ruvB Plasmid, pMTRB—*M. tuberculosis ruvB* (Rv2592c) ORF sequence was obtained on line. The coding sequence corresponding to *ruvB* was PCR-amplified from the cosmid, MTCY 227, using ODNs and was directionally inserted into *pET 21a(+)* expression vector, as described under supplemental "Results and Discussion". The resultant plasmid was designated *pMTRB*.

Purification of M. tuberculosis RuvB—*M. tuberculosis* RuvB was overexpressed in *E. coli* strain Rosetta2(DE3)pLysS harboring the plasmid *pMTRB*. The recombinant RuvB was purified through a series of conventional chromatographic procedures. Details of RuvB protein overexpression and purification are described under supplemental "Results and Discussion". The

purity of *M. tuberculosis* RuvB was >95%, as judged by SDS-PAGE followed by staining with Coomassie Blue (supplemental Fig. 1).

Assays for Survival after UV or MMS Treatment—The sensitivity of *E. coli* Rosetta2 (DE3)pLysS(Δ*ruvB*::*Km*^{R}) cells carrying the vector *pET21a*(+) or *pMTRB* to UV or MMS was examined as described under supplemental "Materials and Methods".

Electrophoretic Mobility Shift Assays—Reaction mixtures (20 μl) contained 20 mM HEPES (pH 7.5), 10 mM $MgCl_2$, 0.25 mM ATPγS, 1 mM DTT, 100 μg/ml BSA, 250 pM of the indicated ^{32}P-labeled DNA, and increasing concentrations of MtRuvB. The assays were performed as described under supplemental Materials and Methods".

Holliday Junction Branch Migration Assay—Each reaction mixture (20 μl) contained 20 mM Tris-HCl (pH 7.5), 10 mM $MgCl_2$, 1 mM ATP, 1 mM DTT, 100 μg/ml BSA, 250 pM of the indicated ^{32}P-labeled DNA, 250 nM MtRuvA, and increasing concentrations of MtRuvB. After incubation at 37 °C for 30 min, the reaction was terminated by the addition of 50 mM EDTA. Reaction products were deproteinized by incubation with SDS (1%) and proteinase K (0.5 μg/μl) at 37 °C for 30 min. Following the addition of 2.5 μl of gel loading dye solution (0.1% (w/v) of bromphenol blue and xylene cyanol in 20% glycerol), samples were electrophoresed on 12% polyacrylamide gel in 44.5 mM Tris borate buffer (pH 8.3) containing 0.5 mM EDTA at 150 V for 14 h at 4 °C. Gels were dried and exposed to the PhosphorImaging screen, and the images were captured using Fuji FLA-9000 PhosphorImager. Bands were quantified in UVI-Tech gel documentation station using UVI-BandMap software (version 97.04) and plotted using Graphpad Prism (version 5.0).

Homologous Fork Reversal Assay—Each reaction mixture (20 μl) contained 20 mM Tris-HCl (pH 7.5), 10 mM $MgCl_2$, 1 mM ATP, 1 mM DTT, 100 μg/ml BSA, 250 pM of the indicated ^{32}P-labeled DNA, 250 nM MtRuvA, and increasing concentrations of MtRuvB. Reaction mixtures were incubated at 37 °C for 30 min and terminated by the addition of 50 mM EDTA. Reaction products were deproteinized by incubation with SDS (1%) and proteinase K (0.5 μg/μl) at 37 °C for 30 min. Following the addition of 2.5 μl of gel loading dye solution (0.1% (w/v) of bromphenol blue and xylene cyanol in 20% glycerol), samples were electrophoresed on 12% polyacrylamide gel in 44.5 mM Tris borate buffer (pH 8.3) containing 0.5 mM EDTA. Gel electrophoresis was carried out at 150 V, for variable times, depending on the fork substrate, at 4 °C. The electrophoresis time was 9, 8.5, 7.5, 7, or 6.5 h for HomFork 44/44, HomFork 44/36, HomFork 44/28, HomFork 44/20, or HomFork 44/16, and HomFork 16/44, respectively. Gels were dried and exposed to the PhosphorImaging screen, and images were captured using Fuji FLA-9000 PhosphorImager. Bands were quantified in a UVI-Tech gel documentation station using UVI-BandMap software (version 97.04) and plotted using Graphpad Prism (version 5.0).

Kinetics of Homologous Fork Reversal—Each reaction mixture (20 μl) contained 20 mM Tris-HCl (pH 7.5), 10 mM $MgCl_2$, 1 mM ATP, 1 mM DTT, 100 μg/ml BSA, 250 pM of the indicated ^{32}P-labeled DNA, 250 nM MtRuvA, and 750 nM MtRuvB. After incubation at 37 °C for the indicated time intervals, the reaction was terminated by the addition of 50 mM EDTA. Reaction products were deproteinized by incubation with SDS (1%) and proteinase K (0.5 μg/μl) at 37 °C for 30 min. After the addition of 2.5 μl of gel loading dye, samples were electrophoresed on 12% polyacrylamide gel in 44.5 mM Tris borate buffer (pH 8.3) containing 0.5 mM EDTA. Gel electrophoresis was performed at 150 V, for variable time depending on the fork substrate, at 4 °C. Electrophoresis run time was 9, 8.5, 7.5, 7, and 6.5 h for HomFork 44/44, HomFork 44/36, HomFork 44/28, HomFork 44/20 or HomFork 44/16, and HomFork 16/44, respectively. Gels were dried and exposed to the PhosphorImaging screen; the images were captured and the bands were quantified in UVI-Tech gel documentation station as described above.

Fork Reversal Assay with Plasmid-based Fork Substrates—Each reaction mixture (20 μl) contained 20 mM Tris-HCl (pH 7.5), 10 mM $MgCl_2$, 2 mM ATP, 1 mM DTT, 100 μg/ml BSA, 1 nM of the indicated ^{32}P-labeled DNA, 1 μM MtRuvA, and increasing concentrations of MtRuvB. After incubation at 37 °C for 30 min, the reactions were terminated by addition of 10 mM ATPγS and subjected to multiple freeze-thaw cycles in liquid nitrogen. One unit of the indicated restriction enzyme was added to the reactions, and incubation was continued at 37 °C for an additional 60-min period. Reaction products were deproteinized by incubation with SDS (1%) and proteinase K (0.5 μg/μl) at 37 °C for 30 min. Following the addition of 3 μl of gel loading dye solution, samples were electrophoresed on 6% polyacrylamide gel (29:1) in 44.5 mM Tris borate buffer (pH 8.3) containing 0.5 mM EDTA at 150 V for 5 h 30 min at 4 °C. Gels were dried and exposed to the PhosphorImaging screen, and images were captured using Fuji FLA-9000 PhosphorImager. Reactions where restriction digestion was carried out with EcoRI, PvuII, or AlwNI alone, the samples were electrophoresed on 6% polyacrylamide gel (29:1) at 150 V for 6, 9, or 11 h, respectively.

In time course reactions with RF substrate, reactions contained 1 μM MtRuvA and 200 nM MtRuvB in the reaction buffer. Reactions were terminated at the indicated time intervals by the addition of 5 mM ATPγS and subjected to multiple freeze-thaw cycles in liquid nitrogen. One unit of the indicated restriction enzyme was added to the reactions, and incubation was continued at 37 °C for additional 60 min. Reaction products were deproteinized and subjected to electrophoresis on 6% polyacrylamide gel. Gels were dried and exposed to the PhosphorImaging screen, and the images were acquired using Fuji FLA-9000 PhosphorImager. The bands were quantified in UVI-Tech gel documentation station using UVI-BandMap software (version 97.04) and plotted using Graphpad Prism (version 5.0).

RESULTS

Bioinformatics—Comparison of the deduced amino acid sequence of MtRuvB with other mycobacterial and eubacterial species revealed that it is evolutionarily related to the family of RuvB proteins (see supplemental Fig. 2 and supplemental Table 3).

Functional Complementation—To ascertain the functional identity of *M. tuberculosis ruvB in vivo*, *E. coli* Δ*ruvB* strain was complemented using the recombinant plasmid, *pMTRB* (see supplemental "Materials and Methods"). Complementation was examined by its ability to confer resistance to genotoxic

stress. The results point toward *M. tuberculosis ruvB* being active in *E. coli* and its ability to make functionally similar contacts with *E. coli* RuvA and RuvC proteins (see supplemental Fig. 3, *A* and *B*).

Purification and Characterization of M. tuberculosis RuvB Protein—Purification of RuvB was carried out by expression from recombinant plasmid *pMTRB* in *E. coli* strain, Rosetta2(DE3)pLysS, as described under supplemental "Results and Discussion".

DNA Binding Activity of MtRuvB in the Presence of Cognate RuvA—As a part of our broader goal to investigate the RFR activity of MtRuvAB complex, we first examined its binding to different substrates that are likely to occur during the processes of DNA replication and/or rescue of stalled replication forks. Activity was assayed in a binding buffer containing a fixed amount of the specified ^{32}P-labeled DNA substrate under the following conditions: (i) in the absence of MtRuvA and MtRuvB; (ii) in the presence of MtRuvA or MtRuvB; and (iii) in the presence of a fixed amount of MtRuvA and increasing concentrations of MtRuvB. Samples were resolved on a 6% polyacrylamide gel as described under "Experimental Procedures." These analyses showed that MtRuvA alone was able to form stable complexes with the HJ, three-way junction, and replication fork intermediates (Fig. 1, *A–C, lane 2*), whereas RuvB alone had little or no measurable DNA binding activity (Fig. 1, *A–C, lane 3*). At higher concentrations of MtRuvB, in the presence of a fixed amount of RuvA, the amount of MtRuvA-DNA complex diminished with a concomitant increase in the amounts of MtRuvAB-HJ, MtRuvAB-three-way junction, and MtRuvAB-RF complexes (Fig. 1, *A–C, lanes 7–14*). Intriguingly, at lower concentrations of RuvB, and in the presence of a fixed amount of RuvA, the amount of protein-DNA complex formed was less than that of MtRuvA alone (Fig. 1, *A–F,* compare *lane 2* with *lanes 4–7*). Although the reason for this is unclear, a plausible explanation would be that some intermediate formed is not resolved from the unbound substrate. Nevertheless, increased amounts of RuvB led to supershifted RuvA-DNA complexes, consistent with previous studies that combined action of *E. coli* RuvA and RuvB resulted in a supershifted RuvA-Holliday junction complex, indicative of the formation of a RuvAB-Holliday junction complex (22). To determine the substrate specificity, similar assays were performed with other known replication or stalled replication intermediates. Although we observed discrete and stable binding between MtRuvB and the indicated substrates, the level of binding was significantly reduced for branched DNA substrates such as 5′ flap, 3′ flap, flayed duplex, and duplex DNA with either 5′ or 3′ overhangs, and no binding to ssDNA, at each concentration of RuvB (Fig. 1, *D--J*). However, MtRuvA alone was able to bind ssDNA (Fig. 1*J, lane 2*). The quantitative data indicate that the substrate specificity of RuvB proceeded in the following order: HJ > three-way junction and replication fork intermediates > linear duplex DNA > 5′ and 3′ flap structure (Fig. 1*K*).

MtRuvAB Promotes Efficient Branch Migration of Homologous but Not of Heterologous Holliday Junctions—The foregoing results showed that MtRuvB exhibited a relatively high binding affinity for the HJ substrate in the presence of RuvA. To further corroborate this finding, we examined the branch migration/resolution activity of MtRuvB using homologous and heterologous HJ substrates. The homologous HJ contained a 4-bp mobile core and 40-bp arm length (Fig. 2*A*, *panel i*), whereas heterologous HJ consisted of a frozen core but of identical arm length (Fig. 2*A*, *panel ii*). Branch migration of the Holliday junctions would generate two dissimilar flayed duplex products depending on the mode of binding of MtRuvB to the pair of symmetrically opposite arms; the flayed duplex generated from ODNs HJO1 and HJO2 migrate faster than the flayed duplex containing HJO1 and HJO4 (Fig. 2, *B* and *C*, *lanes 12* and *13*). MtRuvA alone failed to promote branch migration of either homologous or heterologous HJ (Fig. 2, *B* and *C*, *lane 2*), whereas MtRuvB displayed weak branch migration/resolution activity (Fig. 2, *B* and *C*, *lane 3*). However, a small fixed amount of MtRuvA was able to stimulate the branch migration/resolution of homologous HJ by MtRuvB. The amount of flayed duplex thus formed increased with increasing concentrations of MtRuvB (Fig. 2*B*, *lanes 4–11*). In parallel experiments, we examined the ability of MtRuvB to catalyze branch migration/resolution of heterologous HJ. By comparison, the extent of branch migration/resolution of heterologous HJ occurred more slowly and was significantly *lower* (Fig. 2*C*, *lanes 4–11*). The quantitative data indicate that at the highest concentration of MtRuvB tested, ~35% of heterologous HJ, was converted into flayed duplex compared with 80% in the case of homologous HJ, indicating that branch migration/resolution of heterologous HJs is an energetically less favorable process (Fig. 2*D*).

MtRuvA Facilitates Binding of MtRuvB to Homologous Replication Fork Substrates Bearing Variable Structure at Fork Junction—A previous study that addressed replication fork regression by *E. coli* RuvAB complex used substrate that possessed a small homologous core, and the arms were unequal in length (47). The branch point in the substrate can spontaneously migrate within the homologous core, and the results indicated that RuvAB can unwind the fork substrate in both directions. In contrast, unwinding of heterologous replication fork substrates catalyzed by *E. coli* RuvAB occurred predominantly in a direction opposite that required for fork regression (47). Building on these observations, we constructed a series of stable replication fork substrates in which the lagging and leading parental-daughter arms were entirely homologous. A single noncomplementary nucleotide was introduced on both the parental strands, at the fork junction, to prevent spontaneous branch migration (for additional information, see supplemental "Results and Discussion").

Assays were performed in a binding buffer containing the specified ^{32}P-labeled DNA substrate either with MtRuvA, MtRuvB, or a fixed concentration of MtRuvA plus increasing concentrations of MtRuvB, as described above (Fig. 1). EMSA analysis revealed that unlike MtRuvB, MtRuvA was able to form a complex with different types of fork substrates tested (supplemental Fig. 4, *panels A–F*, compare *lane 2 versus lane 3*), albeit weaker with HomFork 44/20, HomFork 44/16, and HomFork 16/44 substrates (supplemental Fig. 4, *panels D–F*). As the amount of MtRuvB was gradually increased, the intensity of the (fast moving) band corresponding to the MtRuvA-DNA complex diminished with a concomitant increase in the signal

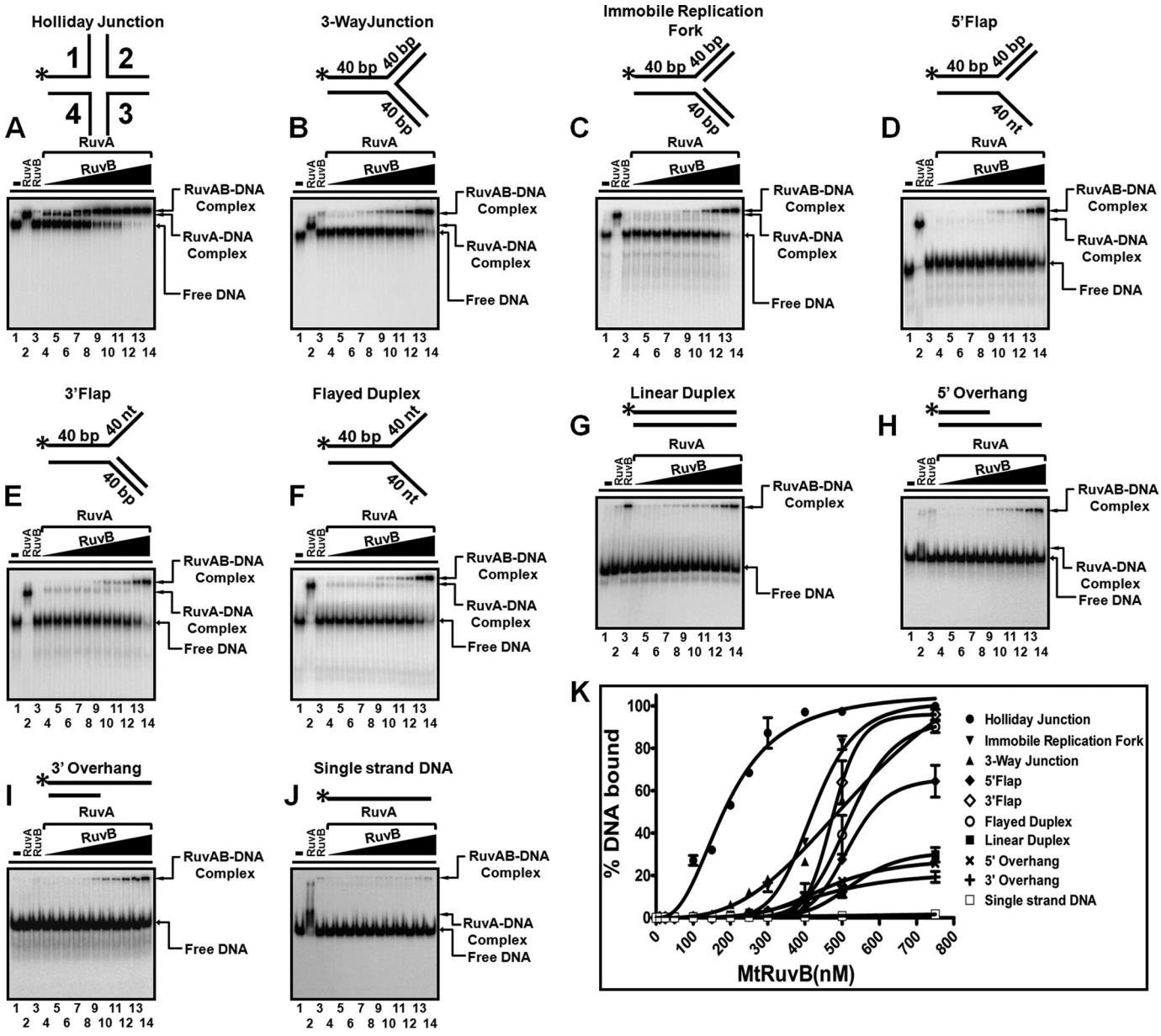

FIGURE 1. **MtRuvAB complex exhibits high affinity for branched DNA substrates.** Each reaction mixture contained 250 pM ^{32}P-labeled DNA substrate (depicted at *top* of each panel) and RuvA, RuvB, or a mixture of both as indicated below. *Lane 1,* DNA substrate alone; *lane 2,* DNA substrate plus 250 nM MtRuvA; and *lane 3,* DNA substrate plus 500 nM MtRuvB. *Lanes 4–14* contained DNA substrate, 250 nM MtRuvA, and 10, 25, 50, 100, 150, 200, 250, 300, 400, 500, or 750 nM MtRuvB, respectively. The *filled triangle* at the *top* of each panel denotes increasing concentrations of MtRuvB. *A,* HJ with homologous core; *B,* three-way junction; *C,* immobile replication fork; *D,* 5′ flap; *E,* 3′ flap; *F,* flayed duplex; *G,* linear duplex DNA; *H,* 3′ overhang; *I,* 5′ overhang; *J,* single-stranded DNA; and *K,* graphical representation of the extent of MtRuvAB binding to different recombination intermediates. The formation of RuvAB-DNA complexes in *A–J* was quantified and plotted as a function of increasing concentrations of MtRuvB. ●, MtRuvA-RuvB-HJ complex; ▲, MtRuvA-RuvB-3-way junction complex; ▼, MtRuvA-RuvB-Immobile replication fork complex; ♦, MtRuvA-RuvB-5′ flap complex; ◇, MtRuvA-RuvB-3′ flap complex; ○, MtRuvA-RuvB-flayed duplex complex; ■, MtRuvA-RuvB linear duplex complex; ×, MtRuvA-RuvB-5′ overhang complex; +, MtRuvA-RuvB-3′ overhang complex; □, MtRuvA-RuvB-ssDNA complex. The *error bars* represent standard deviation of three independent experiments. The data were subjected to nonlinear regression analysis using the equation for one site-specific binding with Hill slope. *Asterisk* refers to the position of radiolabeled phosphate.

intensity of the band corresponding to MtRuvAB-DNA complexes, indicating a synergistic interaction between MtRuvA and MtRuvB (supplemental Fig. 4, *panels A–F, lanes 4–14*). The quantitative data indicate that the differential substrate specificity of RuvB occurred in the following order: HomFork 44/44 > HomFork 16/44 > HomFork 44/36 > HomFork 44/28 > HomFork 44/20 and HomFork 44/16 (supplemental Fig. 4*G*).

MtRuvA and MtRuvB Function Coordinately to Unwind Replication Forks—We have shown in an earlier study that *M. tuberculosis ruvA* was able to complement survival of *E. coli* Δ*ruvA* strain against genotoxic stress (26). Likewise, we found that *M. tuberculosis ruvB* was able to complement survival of *E. coli* Δ*ruvB* cells against UV and MMS-induced stress (supplemental Fig. 3). Analogous studies in *E. coli* suggest that *ruvA ruvB* catalyze fork reversal in strains bearing

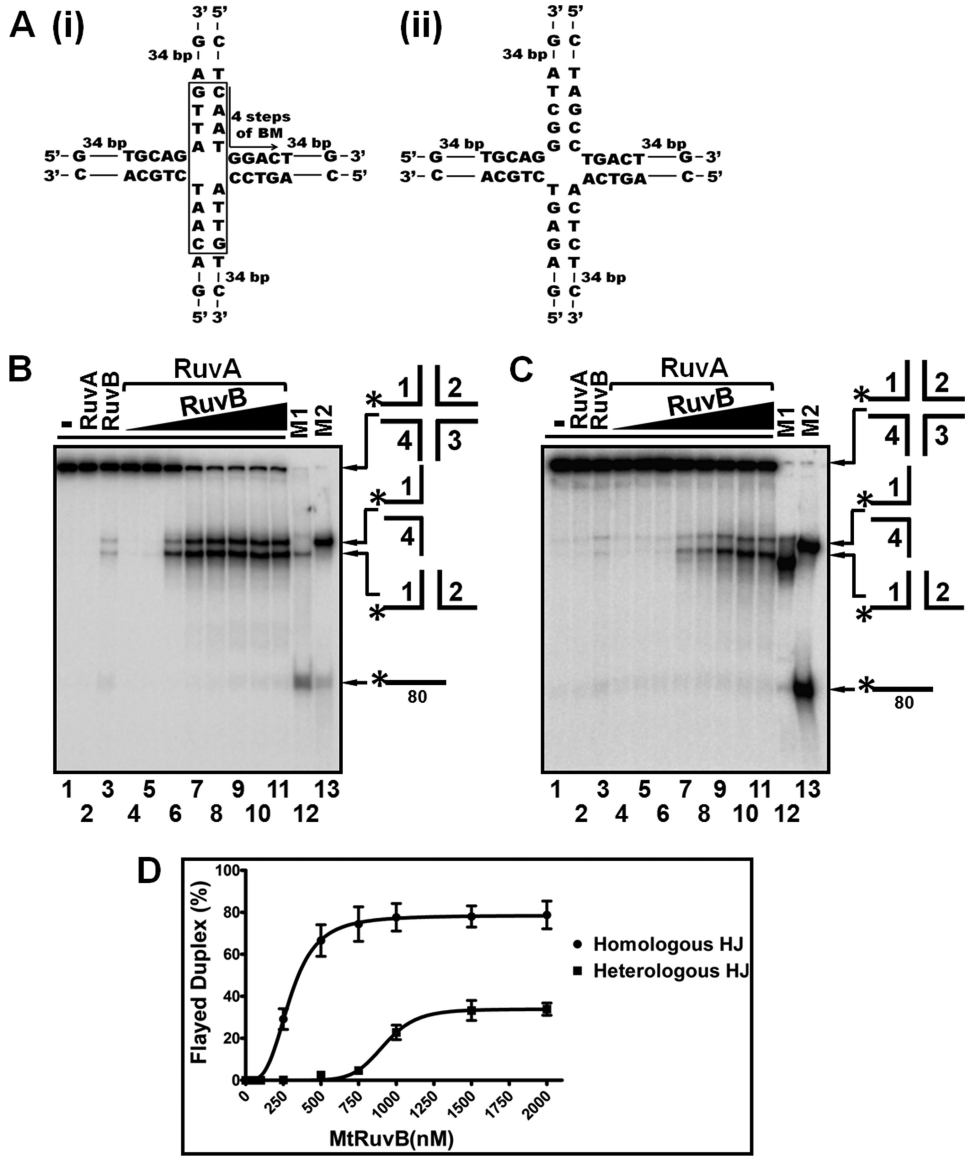

FIGURE 2. **MtRuvAB promotes efficient branch migration of homologous but not of heterologous Holliday junctions.** Each reaction mixture contained 250 pM ^{32}P-labeled substrate and RuvA, RuvB, or a mixture of both as indicated below. *Lane 1,* DNA substrate alone; *lane 2*, DNA substrate plus 250 nM MtRuvA; and *lane 3,* DNA substrate plus 2 μM MtRuvB. *Lanes 4–11* contained substrate plus 250 nM MtRuvA and 50, 100, 250, 500, 750, 1000, 1500, or 2000 nM MtRuvB, respectively. *Lane 12* (M1) contained flayed duplex marker assembled from HJO1 and HJO2, and *lane 13* (M2) contained flayed duplex marker assembled from HJO1 and HJO4. The *filled triangle* at the *top* of each panel denotes increasing concentrations of MtRuvB. *A, panel i,* schematic diagram of homologous, and *panel ii,* heterologous Holliday junctions; *B,* branch migration of homologous Holliday junction; *C,* branch migration of heterologous Holliday junction, and *D,* graphical representation of the amount of the product (flayed duplex) formed in *B* and *C* was quantified and plotted as a function of increasing concentrations of MtRuvB. ●, homologous Holliday junction; ■, Heterologous Holliday junction. Each *point* on the graph represents the mean value of the experiment done in triplicate, and *error bars* represent standard deviation. The best fit curve was obtained by subjecting the data sets to nonlinear regression analysis, in GraphPad PRISM (version 5.00), using the built-in equation for allosteric sigmoidal enzyme kinetics. *Asterisk* refers to the position of radiolabeled phosphate.

defects in replisome components or Rep helicase (15, 37, 38). Previously, other researchers have shown that RuvAB can unwind model replication forks *in vitro*, consistent with the known polarity of regression (3). However, the directionality was limited to DNA substrates in which loading of RuvB was constrained to the parental duplex DNA. Unbiased loading of RuvB resulted in RuvAB-mediated unwinding rather than reannealing of the strands of parental duplex arm (47). It is likely that these inference(s) may be limited by substrate selectivity and, more importantly, unlikely to represent all the potential fork structures *in vivo*. The discrepancies between these results can be attributed to differences in the length of parental and daughter arms of these substrates. Three lines of investigations support this interpretation. One, RuvB normally forms a complex with HJ arms having a minimum length in the range of 24–27 bp (49). Second, asymmetric binding of RuvA tetramer at the Y-junction directs the assembly of a single hexameric RuvB ring onto parental duplex, thereby leading to unidirectional unwinding of these substrates (50). Finally, studies on *E. coli ruvA ruvB* strains that are specifically impaired for fork reversal, but proficient in HR, imply that the function of RuvAB in RFR is genetically separable from its role in branch migration of Holliday junctions (37, 38).

To test these predictions, we performed RFR assays in the presence of MtRuvAB using homologous replication fork substrates. Although DNA helicases have the ability to unwind replication fork substrates leading to the formation of either partial replication forks, parental-daughter partial duplexes, or parental-duplex with unpaired nascent daughter strands, the intermediates so generated will not be favorable for the replication fork reversal process (supplemental Fig. 5, schemes 1–6). In contrast, a DNA helicase catalyzing fork reversal will cause coordinated unwinding of both the parental-daughter duplex arms leading to reannealing of parental strands as well as concomitant annealing of nascent daughter strands to generate an HJ intermediate (supplemental Fig. 5, schemes 7 and 8). The HJ intermediate may be subsequently resolved into parental and daughter duplexes.

We next performed the assay using a homologous fork substrate having a 49-bp parental duplex region and a 44-bp leading and lagging parental-daughter duplex arms (Fig. 3*A*), as described under "Experimental Procedures." Our results revealed that, in the presence of either MtRuvA or MtRuvB, the parental and daughter duplexes were present in similar amounts and seemed to match the background levels, which correspond to about 10% of total input substrate concentration (Fig. 3*A*, compare *lane 4* with *lanes 5* and *6*). The parental and daughter duplexes formed following RFR co-migrated with parental duplex and daughter duplex markers, respectively (Fig. 3*A*, compare *lane 3* with *lanes 7–14*). The background noise (Fig. 3*A*, *lane 4*) and the observed signals in the presence of either MtRuvA or MtRuvB (Fig. 3*A*, *lanes 5* and *6*) may be due to spontaneous dissociation of the shorter duplex. In analogous experiments performed with increasing concentrations of RuvB and a fixed amount of RuvA, we observed increased formation of both parental and daughter duplexes, indicating that RuvA and RuvB coordinately catalyze the RFR reaction (Fig. 3*A*, *lanes 7–14*). To further characterize RFR catalyzed by MtRuvAB, similar assays were performed with replication fork substrates having 36-, 28-, or 20-bp double-stranded regions in the lagging daughter duplex arm. The results depicted in Fig. 3, *B–D, lanes 7–14*, show that MtRuvAB complex catalyzed RFR reaction in a concentration-dependent manner. However, with substrates containing 16 bp in the leading or lagging parental-daughter duplex arms, the extent of MtRuvB-catalyzed conversion to parental and daughter duplexes was not obvious, due to high levels of background noise (Fig. 3, *E* and *F*, compare *lane 4* with *lanes 7–14*). However, irrespective of the nature of the substrate used, the extent of the formation of both parental and daughter duplexes increased with increasing concentrations of MtRuvB (Fig. 3, *A–F, lanes 7–14*). Quantification of RFR reaction products revealed that the efficiency of the formation of daughter duplexes is slightly higher than that of parental duplexes (Fig. 3, *G* and *H*).

MtRuvAB Catalyzes Coordinated Unwinding and Annealing of Daughter Strands of Homologous Fork Substrates—In a *bona fide* RFR reaction, the released fragments will carry the originally labeled 5′ terminus and will be double-stranded (51). Although spontaneous dissociation of the parental-daughter partial duplexes followed by annealing of the parental strands might regenerate the parental duplex, the appearance of the daughter duplex can be rationalized only by coordinated unwinding and annealing of the daughter strands of both the parental-daughter arms. Thus, the appearance of daughter duplex is an indicator of a *bona fide* fork reversal reaction.

To gain insights into the relative rates of RFR, we examined the time course of MtRuvAB-catalyzed formation of parental and daughter duplexes. Assays were performed in the presence of a fixed amount of MtRuvA and MtRuvB. The amount of daughter duplex increased with time and with similar efficiencies, and the reactions were essentially complete within 12 min (Fig. 4, *A–F, lanes 8–14*). Furthermore, the formation of lagging daughter strand was minimal over the same time period, indicating that the strands are simultaneously unwound and annealed to produce daughter duplexes (Fig. 4, *A–F, lanes 8–14*). To further corroborate these findings with respect to the appearance of daughter duplex, we performed control reactions with daughter strands (Fig. 4, *A–F,* compare *lanes 3* and *4*). Quantification of RFR reaction products revealed that the rates and the overall efficiency of the formation of daughter duplexes are slightly higher than that of parental duplexes (Fig. 4, *G* and *H,* and supplemental Table 4). Altogether, these results are consistent with the notion that the MtRuvAB complex can efficiently catalyze *in vitro* replication fork reversal reaction on homologous fork substrates.

Extent of RFR Is Dependent on RuvB Concentration—Under *in vivo* conditions, uncoupling or impairment of leading and lagging strand synthesis will lead to the formation of inactivated replication forks and consequently produce a substrate for RuvABC complex at the replication forks (52–54). To examine the role of MtRuvAB in processing of stalled replication forks at chromosome level, assays were performed using plasmid-derived model "RF" substrate. This substrate mimics the stalled replication fork in which the lagging daughter strand is 14 nucleotides longer than the leading daughter strand (55). The reaction was monitored for the appearance of a labeled DNA fragment generated from the extruded arm by the indicated restriction enzyme (Fig. 5*A*).

The plasmid-derived model RF substrate (preparation of the substrate depicted in supplemental Fig. 7) was incubated either with MtRuvA, MtRuvB, or both and then digested with EcoRI (Fig. 5*B*, *panel I*) or PvuII (Fig. 5*B*, *panel II*). The reaction products were then separated by PAGE and visualized as described above. As shown in Fig. 5*B* (*panels I* and *II, lanes 4* and *5*), either MtRuvA or MtRuvB was unable to cause any significant increase in product levels over the background noise. However, incubation with increasing concentrations of RuvB, in the presence of a fixed amount of RuvA, resulted in a concomitant increase in the amounts of 86- or 266-bp labeled fragments corresponding to the 5′-end of the reversed arm, respectively (Fig. 5*B*, *panels I* and *II*, *lanes 6–13*). Notably, at the highest RuvB concentration tested, 80% of molecules (from the total input DNA) contained the reversed arm (Fig. 5*B*, *panels I* and *II, lane 13*).

The identity of the DNA fragments was confirmed by subjecting them to restriction digestion with an enzyme whose site lies between the 5′-end and the initial restriction enzyme used to release the fragment. Initially, the reversal was monitored by treating the reaction products with EcoRI, which resulted in the

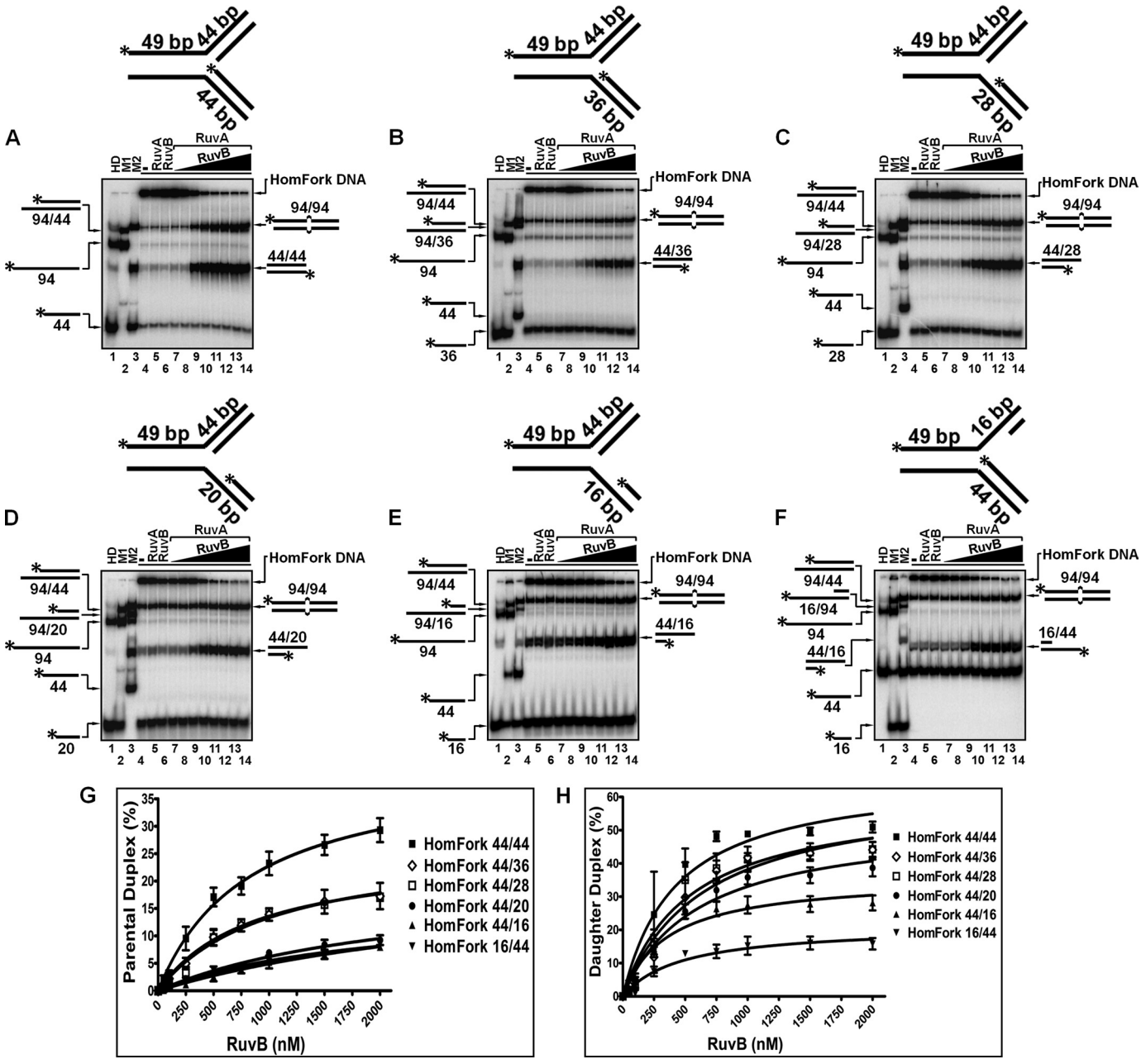

FIGURE 3. **MtRuvA and MtRuvB act coordinately to catalyze RFR on substrates bearing variable structure at fork junction.** Each reaction mixture contained 250 pM ^{32}P-labeled DNA substrate (depicted at the *top* of each panel) and RuvA, RuvB or a mixture of both as indicated below. *Lane 1,* heat-denatured (*HD*) substrate; *lane 2, M1*; and *lane 3, M2* contain duplex, partial duplex, and ssDNA markers. *Lane 4,* DNA substrate alone; *lane 5,* DNA substrate plus 250 nM MtRuvA; *lane 6,* DNA substrate plus 2 μM MtRuvB. *Lanes 7–14* contained DNA substrate plus 250 nM MtRuvA and 50, 100, 250, 500, 750, 1000, 1500, and 2000 nM MtRuvB, respectively. The *filled triangle* at the *top* of each panel denotes increasing concentrations of MtRuvB. *A,* HomFork 44/44; *B,* HomFork 44/36; *C,* HomFork 44/28; *D,* HomFork 44/420; *E,* HomFork 44/16; and *F,* HomFork 16/44. *G* and *H* show graphical representation of the efficiency of formation of parental and daughter duplex products, respectively. *A–F*, intensity of the bands corresponding to the parental and daughter duplex products was quantified, and the background noise corresponding to parental and daughter duplex products in *lane 4* was subtracted from each value. The amount of parental and daughter duplex generated in the reaction was plotted as a function of increasing concentrations of MtRuvB. Each *point* on the graph represents the mean value of the experiment done in triplicate, and *error bars* represent standard deviation. The best fit curve was obtained by subjecting the data sets to nonlinear regression analysis, in GraphPad PRISM (version 5.00), using the built-in equation for Michaelis-Menten enzyme kinetics. *Asterisk* refers to the position of radiolabeled phosphate.

release of the 86-bp fragment (Fig. 5*C*, *lane 9*). This fragment, upon subsequent digestion with AvrII or BamHI, led to the release of 5′-end-labeled 36- or 61-bp fragments, respectively. The mobility of these secondary fragments is identical to the mobility of duplexes generated by the action of AvrII or BamHI on the products of a fork reversal reaction (Fig. 5*C*, compare *lane 7* with *11* and *lane 8* with *10*).

MtRuvAB-catalyzed Extensive Fork Reversal Is Dependent on ATP Hydrolysis—The sequential transfer of restriction endonuclease cleavage sites from the daughter strand to the extruded arm provides a sensitive assay to measure the extent of RFR under *in vitro* conditions (Fig. 6*A*). Digesting the extruded arm with different restriction enzymes will lead to the generation of duplex fragments of specific size. Accordingly, the

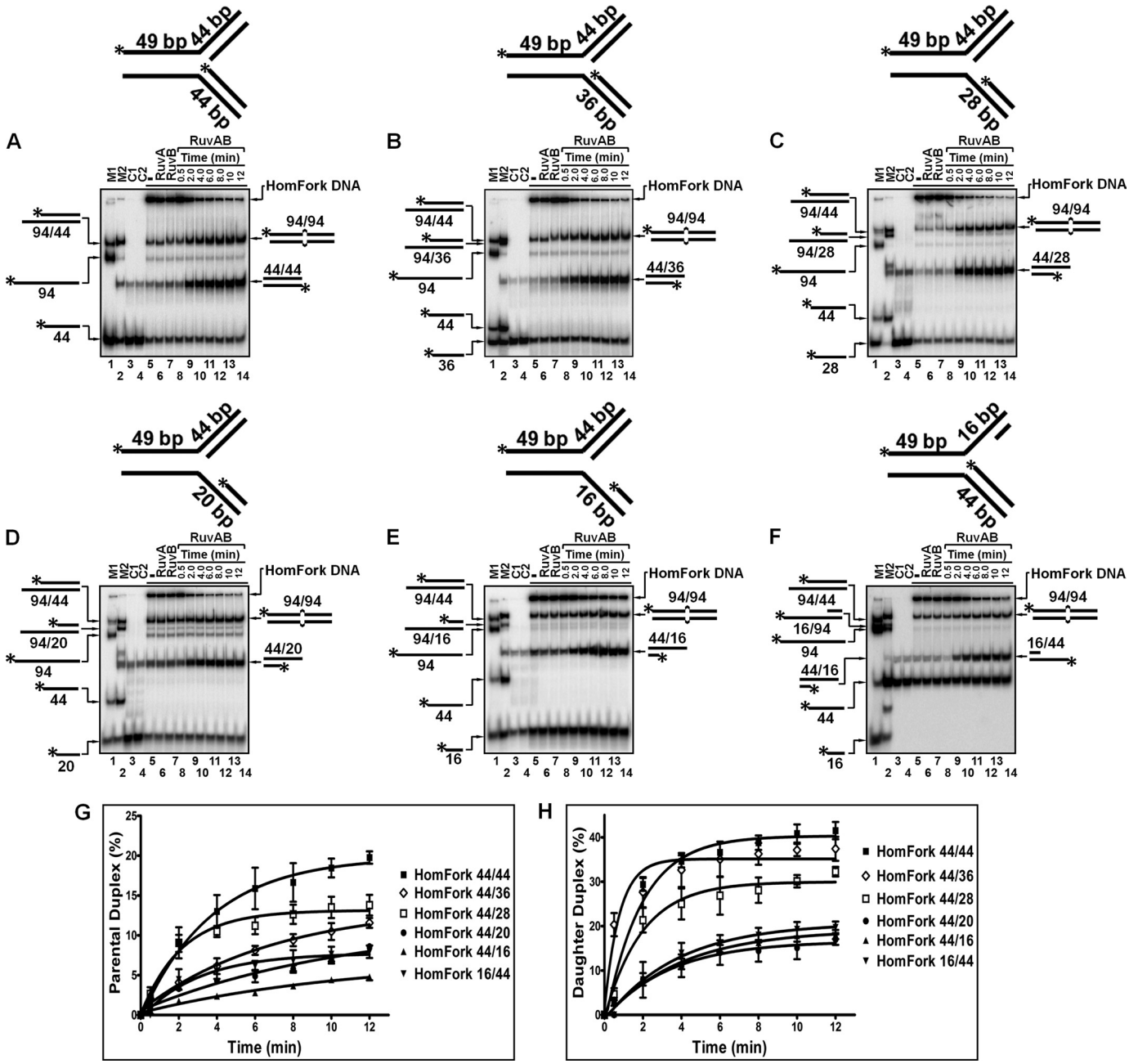

FIGURE 4. **MtRuvAB catalyzes coordinated unwinding and annealing of daughter strands of homologous fork substrates as a function of time.** Each reaction mixture contained 250 pM ^{32}P-labeled DNA substrate (as depicted at the *top* of each panel) plus RuvA, RuvB, or a mixture of both as indicated. *Lane 1* (M1) and *lane 2* (M2) contain duplex, partial duplex, and ssDNA markers. *Lane 3* (C1) contained 250 pM ODN DLead 44. *A–E* contained 250 pM ^{32}P-labeled DLag 44, 36, 28, 20, or 16, respectively. *F, lane 3* (C1) contained 250 pM ODN DLead 16 and 250 pM ^{32}P-labeled DLag 44. *Lane 4* (C2), in *A–F*, contained DNA oligonucleotides as indicated for *lane 3* except that reaction buffer contained 250 nM MtRuvA and 750 nM MtRuvB. *Lane 5,* 250 pM substrate; *lane 6*, substrate in the presence of 250 nM MtRuvA, and *lane 7*, substrate in the presence of 2 μM MtRuvB. *Lanes 8–14* contained substrate plus 250 nM MtRuvA and 750 nM MtRuvB. *A–F*, *lanes 8–14*, the time points (in min) for the reactions are shown at the *top* of each lane. *A*, HomFork 44/44; *B,* HomFork 44/36; *C,* HomFork 44/28; *D,* HomFork 44/20; *E,* HomFork 44/16; and *F,* HomFork 16/44. *G* and *H* show graphical representation of the efficiency of formation of parental and daughter duplex products, respectively. *A–F*, the bands corresponding to the parental and daughter duplex products was quantified, and the background noise corresponding to parental and daughter duplex products in *lane 5* was subtracted from each value. The amount of parental and daughter duplex generated in the reaction was plotted as a function of time. Each *point* on the graph represents the mean value of experiment done in triplicate, and *error bars* represent standard deviation. The best fit curve was obtained by subjecting the data sets to nonlinear regression analysis, in GraphPad PRISM (version 5.00), using the built-in equation for one-phase exponential association. *Asterisk* refers to the position of radiolabeled phosphate.

extent of fork reversal catalyzed by MtRuvAB can be determined by the appearance of a series of DNA fragments of increasing length. In control reactions, performed in the absence of MtRuvAB, we found weak RFR activity, perhaps because of the spontaneous branch migration of the RF substrate. In all these lanes, we observed weak bands corresponding to the expected sizes of DNA fragments (Fig. 6*B*, *lanes 3–8*). Parallel experiments were performed to ascertain the role of ATP hydrolysis in RFR reactions catalyzed by the MtRuvAB complex. In the presence of ATPγS, the RFR activity catalyzed by MtRuvAB was similar to that observed in control reactions (compare Fig. 6, *C*, *lanes 3–8*, with *B*, *lanes 3–8*). However,

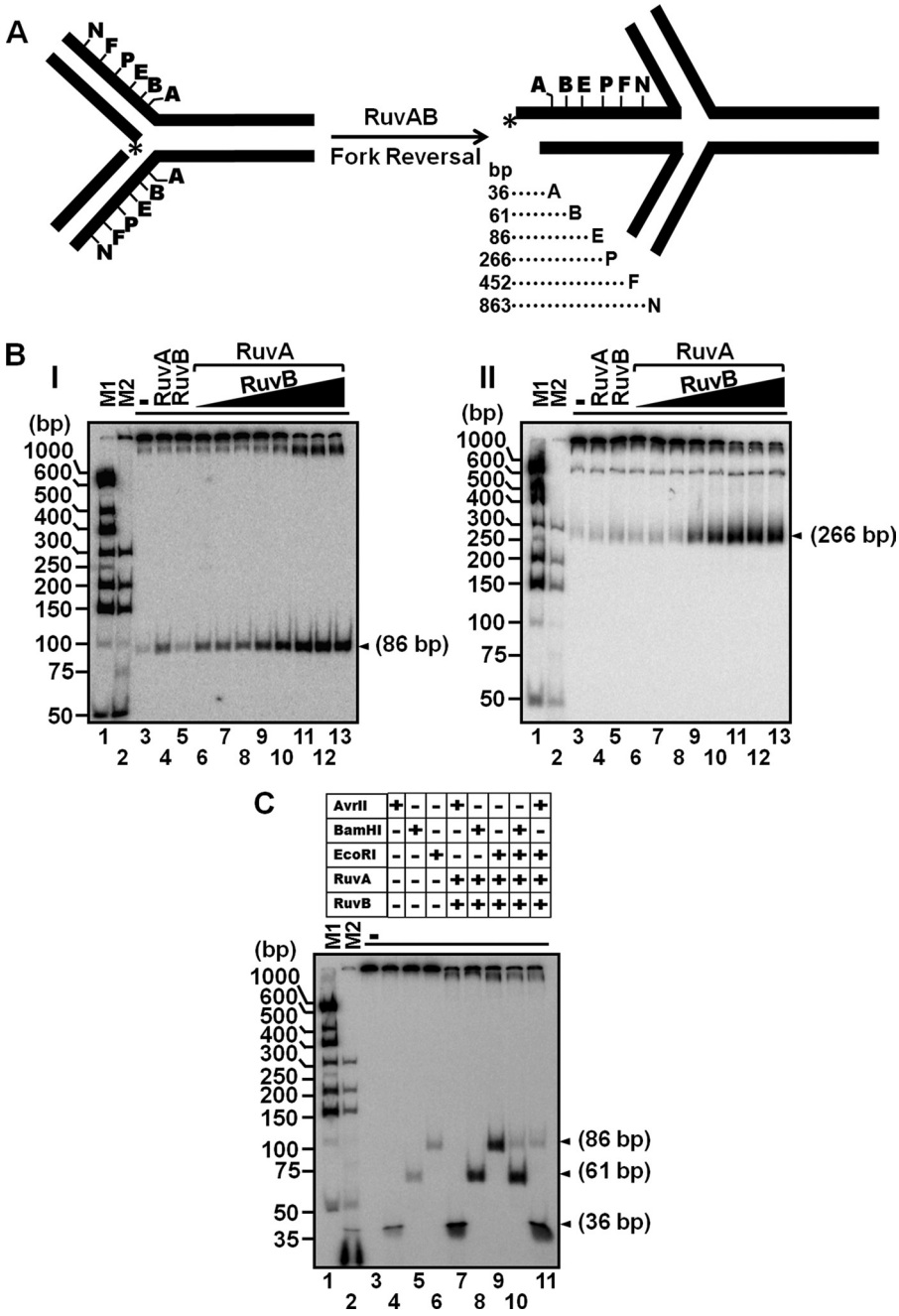

FIGURE 5. **Extent of RFR is dependent on RuvB concentration.** *A,* schematic diagram of the RFR reaction depicting the appearance of the reversed arm. Restriction enzyme cleavage sites are indicated by the following letters: *A,* AvrII; *B,* BamHI; *E,* EcoRI; *P,* PvuII; *F,* AflIII and *N,* AlwnI. *Asterisk* indicates the ^{32}P-labeled 5′-end of lagging daughter strand. *Below* the RFR product in the diagram, the sizes of different branches in base pairs are indicated. *B,* analysis of products generated by EcoRI or PvuII digestion. Each reaction mixture contained 1 nM ^{32}P-labeled RF substrate (*lane 3*) and in the presence of 1000 nM MtRuvA (*lane 4*) or 200 nM MtRuvB (*lane 3*). *Lanes 6–13* contain 1 nM substrate in the presence of 1000 nM MtRuvA and 10, 25, 50, 75, 100, 150, 200, or 250 nM MtRuvB, respectively. The *filled triangle* at the *top* of each panel denotes increasing concentrations of MtRuvB. *Lanes 1* and *2* (*M1* and *M2*) contain ^{32}P-labeled Gene Ruler 50-bp DNA ladder or ^{32}P-labeled Gene Ruler ultra low range DNA ladder, respectively. *Panel I* shows fragment released by EcoRI digestion of the reversed arm; *panel II* shows fragment released by PvuII digestion of the reversed arm. *C,* confirmation of RuvAB-mediated reversal of RF substrate. Reaction mixtures contained 1 nM ^{32}P-labeled replication fork substrate in the absence of RuvAB (*lanes 4–6*) or in the presence of 1000 nM MtRuvA and 200 nM MtRuvB (*lanes 7–11*), respectively. *Lanes 4–6,* products generated by cleavage with AvrII, BamHI, or EcoRI. *Lanes 7–9,* products generated by AvrII, BamHI, or EcoRI in the presence of MtRuvAB. The EcoRI-digested product was subsequently digested by either BamHI or AvrII (*lanes 10* and *11*, respectively). *Lane 1* (*M1*) and *lane 2* (*M2*) contain ^{32}P-labeled Gene Ruler 50-bp DNA ladder and ^{32}P-labeled Gene Ruler ultra low range DNA ladder, respectively.

substitution of ATP for ATPγS led to a significant increase in the amount of the same DNA fragments, indicating that MtRuvAB-catalyzed RFR is coupled to ATP hydrolysis (Fig. 6*C*, compare *lanes 3–8* with *9–14*). We note that the extent of MtRuvAB-catalyzed *in vitro* RFR is comparable with fork regression observed in mammalian cells (56).

To ascertain the ability of MtRuvAB to catalyze complete fork reversal, the RFR reaction was performed using a JM substrate that was constructed by annealing a gapped circular plasmid and homologous linear duplex bearing complementary single-stranded gaps (depicted in Fig. 6*D*). The gapped circular plasmid was labeled at the 5′-end. Complete fork reversal on a

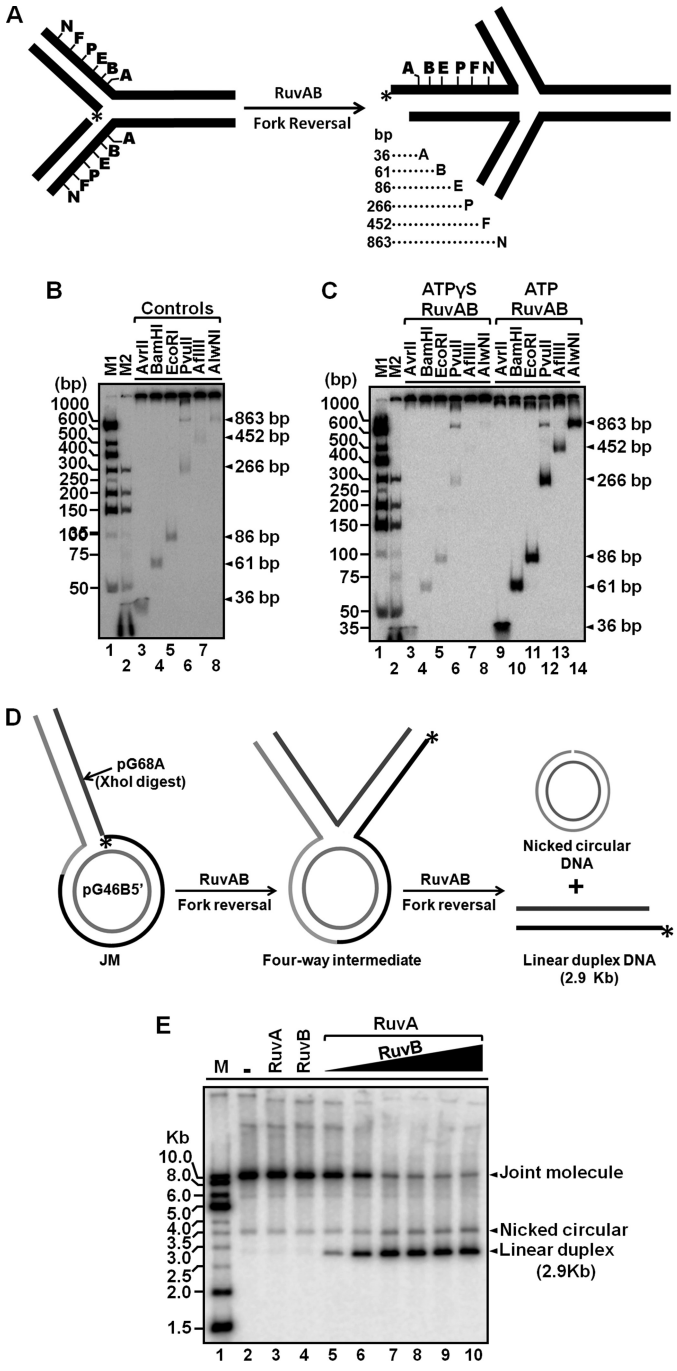

FIGURE 6. **MtRuvAB catalyzes extensive fork reversal in an ATP hydrolysis-dependent reaction.** *A,* schematic diagram of the DNA substrate and the outcome of MtRuvAB-catalyzed RFR reaction. Restriction enzyme cleavage sites are indicated by the following letters: *A,* AvrII; *B,* BamHI; *E,* EcoRI; *P,* PvuII; *F,* AflIII, and *N,* AlwnI. *Asterisk* indicates the ^{32}P-labeled 5′-end of lagging daughter strand. *Below* the RFR product in the diagram, the sizes of different branches in base pairs are indicated. *B,* analysis of the extent of RFR in the absence of MtRuvAB but in the presence of 2 mM ATP. *Lane 1* (*M1*) and *lane 2* (*M2*) show ^{32}P-labeled Gene Ruler 50-bp DNA ladder, and ^{32}P-labeled Gene Ruler ultra low range DNA ladder, respectively. *Lanes 3–8* show the restriction fragments generated in the control reactions in the absence of MtRuvAB. *C,* analysis of MtRuvAB-catalyzed RFR activity monitored in the presence of ATPγS or ATP. The assay was performed using ^{32}P-labeled RF substrate (1 nM) and indicated nucleotide cofactor (2 mM) in the presence of a fixed amount of MtRuvA (1000 nM) and MtRuvB (200 nM). The different restriction enzymes used are indicated at the *top* of each lane, and the size of different products generated by restriction endonucleases is shown on the *right side* of the gel image. *Lane 1* (*M1*) and *lane 2* (*M2*) show ^{32}P-labeled Gene Ruler 50-bp DNA ladder, and ^{32}P-labeled Gene Ruler ultra low range DNA ladder, respectively. *Lanes 3–8* show the restriction fragments generated in presence of ATPγS and MtRuvAB, and *lanes 9–14* show restriction fragments released subsequent to fork reversal by MtRuvAB in the presence of ATP. *D,* schematic diagram of the homologous JM substrate and the outcome of RuvAB-mediated fork reversal reaction. Complete fork reversal results in the formation of 5′-end-labeled linear duplex DNA (2.9 kb) and nicked circular DNA. *Asterisk* indicates the ^{32}P-labeled 5′-end of lagging daughter strand. *E,* agarose gel analysis of complete fork reversal catalyzed by MtRuvAB. *Lane 1,* ^{32}P-labeled 1-kb DNA ladder; *lane 2,* 1 nM ^{32}P-labeled JM substrate alone; *lanes 3* and *4*, 1 nM ^{32}P-labeled JM substrate in the presence of 1000 nM MtRuvA or in presence of 600 nM MtRuvB, respectively. *Lanes 5–10,* 1 nM ^{32}P-labeled JM substrate in the presence of 1000 nM MtRuvA and 100, 200, 300, 400, 500, or 600 nM MtRuvB, respectively. The *filled triangle* at the *top* of the gel image denotes increasing concentrations of MtRuvB. Position of JM substrate, nicked circular, and linear duplex DNA is indicated.

homologous JM would result in the formation of a linear duplex and nicked circular DNA products due to the simultaneous transfer of labeled strand from the circular plasmid context to the 2.9-kb linear duplex DNA (Fig. 6*D*). To ascertain if fork reversal proceeded to completion, we incubated the JM substrate with increasing concentrations of MtRuvB in the presence of a fixed amount of RuvA. Reaction products were resolved by electrophoresis on an agarose gel. As shown in Fig. 6*E*, *lanes 3* and *4*, MtRuvA or MtRuvB alone was unable to catalyze the reversal reaction. Increasing concentrations of MtRuvB, in the presence of a fixed amount of MtRuvA, led to an increase in the extent of accumulation of the expected 2.9-kb linear DNA fragment (Fig. 6*E*, *lanes 5–10*), thus indicating that the reaction proceeds virtually to completion.

MtRuvAB-catalyzed Replication Fork Reversal Is Progressive—The progressive nature of RFR catalyzed by MtRuvAB was ascertained by monitoring the extent of fork reversal over an extended period of time, using EcoRI and PvuII cleavage sites that are 180 bp apart in the context of the reversed arm (Fig. 7*A*). In a progressive fork reversal reaction, the proximal EcoRI site is expected to be transferred into the extruded arm first, compared with the distal PvuII site. To confirm this, the RF substrate was incubated with a fixed concentration of RuvAB complex. The reactions were terminated at the indicated time points, and the reaction mixtures were analyzed by PAGE. The DNA fragments produced by EcoRI digestion appeared as early as 3 min, whereas the PvuII-digested fragments appeared at 6 min (Fig. 7*B*, compare *panel I, lane 4 versus panel II, lane 5*). Furthermore, quantification of results shown in Fig. 7*B* (*panels I* and *II*) suggested that RFR catalyzed by the MtRuvAB complex occurred in a progressive manner (Fig. 7*C*).

MtRuvAB-catalyzed RFR Is Uncoupled from DNA Supercoiling—In partially replicated plasmids, positive topological stress is relieved exclusively by reversal of the replication fork leading to re-annealing of parental strands and subsequent base pairing of the daughter strands (57). The translocation of RuvB helicase along the circular RF substrate might introduce supercoils in the substrate that might, in turn, indirectly cause fork reversal. To eliminate the possibility of supercoiling being the driving force behind MtRuvAB-catalyzed replication fork reversal, the RF substrate was linearized by HindIII digestion and subsequently used in the fork reversal assay (Fig. 8*A*). The linear nature of the DNA substrate ensures that it cannot accumulate any supercoils because of the translocation of RuvAB complex. We found that MtRuvAB was able to efficiently

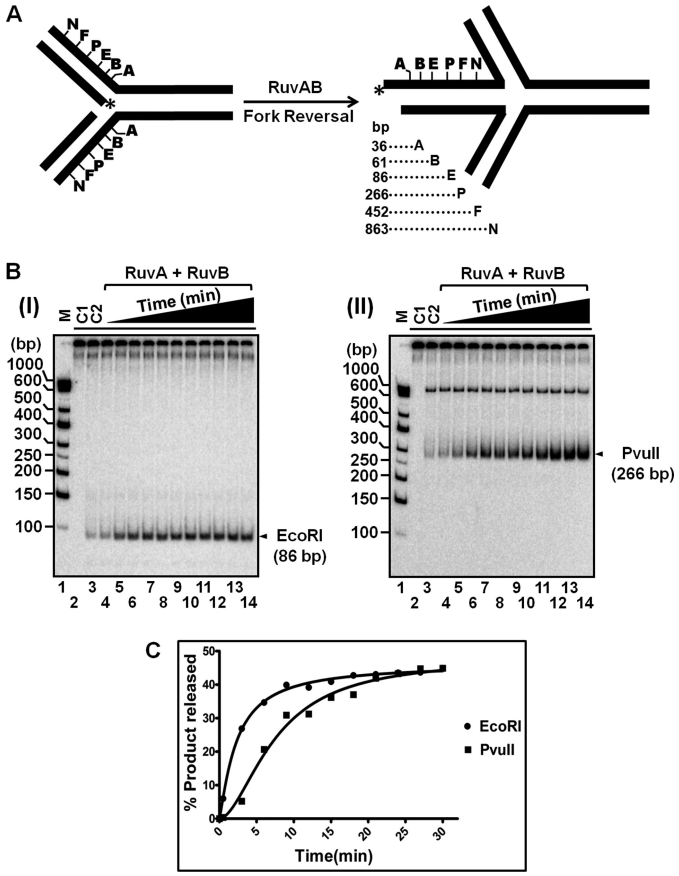

FIGURE 7. **RFR catalyzed by MtRuvAB is progressive.** *A,* schematic diagram of the DNA substrate and the outcome of RFR reaction. *Below* the RFR product in the diagram, the sizes of different branches in base pairs are indicated. *Asterisk* refers to the position of radiolabeled phosphate on the 5′-end of the lagging daughter strand. *B, panel I,* time course of RFR as monitored by restriction enzyme digestion with EcoRI. *B, panel II,* time course of RFR as monitored by restriction enzyme digestion with PvuII. *Lane 1,* ^{32}P-labeled Gene Ruler 50 bp of DNA ladder; *lane 2* (*C1*), each reaction mixture contained 1 nM ^{32}P-labeled substrate alone, and *lane 3* (*C2*), in the absence of RuvAB, but treated with EcoRI. *Lanes 4–14,* containing 1 nM ^{32}P-labeled substrate with 1000 nM RuvA and 250 nM RuvB were incubated for 0.5, 3, 6, 9, 12, 15, 18, 21, 24, 27, or 30 min, respectively. Restriction endonuclease cleavage sites are indicated by the following letters: *E,* EcoRI, and *P,* PvuII. The *filled triangle* at the *top* of the gel image denotes increasing time. *C,* graphical representation of the extent of product formation. The bands in *B, panels I* and *II,* were quantified and plotted as a function of time. Each *point* on the graph represents the mean value of experiment done in duplicate. The best fit curve was obtained by subjecting the data sets to nonlinear regression analysis, in GraphPad PRISM (version 5.00), using the built-in equation for allosteric sigmoidal enzyme kinetics. ●, EcoRI digestion released fragments; ■, PvuII digestion released fragments.

reverse the fork in the RF/HindIII substrate (Fig. 8*B, lanes 6–11*), consistent with the notion that the generation of positive torsional stress in the RF substrate is not responsible for the observed fork reversal activity of MtRuvAB complex.

MtRuvAB-catalyzed RFR Is Not Impeded by a Short Heterologous Sequence—Previously, others have shown that a 20-bp heterologous insert blocked branch migration of HJ catalyzed by the *E. coli* RuvAB complex (58). To explore if MtRuvAB-catalyzed RFR can bypass small regions of heterology, we generated a plasmid-based JM bearing 29-bp heterologous insert at the SapI site in the leading arm (supplemental Fig. 6*B*) (59). We postulated that if MtRuvAB can drive RFR through heterologous insertions, it would result in the creation of unique cleavage sites for AvrII, BamHI, EcoRI, SapI, AflIII, and AlwnI in the reversed arm. Conversely, if fork reversal is impeded by the heterologous insert, the formation of the reversed arm will be blocked beyond the site of insert, thus leading to the absence of the corresponding restriction fragments. For direct comparison, we used a JM substrate without the heterologous insert (supplemental Fig. 6*A*). We incubated radiolabeled JMs with or without the heterologous insert and in the absence or presence of MtRuvAB. The reaction products were digested with the indicated restriction enzyme and analyzed as described under "Experimental Procedures." In reactions performed in the absence of MtRuvAB, we observed a low level of RFR activity with both the substrates, probably because of spontaneous branch migration (Fig. 9, *I* and *II, lanes 3–8*). In the presence of MtRuvAB, however, the RFR activity was higher and similar in magnitude for both the substrates (Fig. 9, compare *lanes 9–14* in *I* with *lanes 9–14* in *II*). Also, the restriction fragment encompassing SapI site could be seen in reaction performed with both the substrates (Fig. 9, *I* and *II, lane 10*). Of note, the AflIII and AlwnI restriction fragments released subsequent to fork reversal of the JM-containing heterologous insert exhibited aberrant electrophoretic mobility when compared with similar fragments derived from the homologous JM substrate (Fig. 9, compare *I* with *II, lanes 11* and *12*). However, unlike the RFR catalyzed by *Saccharomyces cerevisiae* Rad5 (59), our results reveal that a short heterologous insert does not impede the RFR activity catalyzed by MtRuvAB.

DISCUSSION

In this study, we show that the MtRuvAB complex catalyzes branch migration of homologous and heterologous HJs as well as reversal of a variety of homologous fork substrates. We also show that MtRuvAB drives complete fork reversal, in a processive manner, resulting in the generation of a 2.9-kb reversed arm. Notably, MtRuvAB-catalyzed RFR, unlike *E. coli* RuvAB (47), leads to the formation of HJ, and sequence heterology failed to impede its RFR activity. Altogether, these results provide mechanistic insights into the functional role of the MtRuvAB complex in the processing of stalled replication forks *in vivo*.

Studies with mammalian cells led to the concept of replication fork collapse and that the stalled replication forks can be isomerized into an HJ with a DNA double strand end, thereby allowing DNA repair and then continuation of replication (56). Genetic analyses in *E. coli* and bacteriophages disclosed a role for HR pathway in the repair of damaged DNA (60–64). Since then, numerous studies have shown the occurrence of such structures, which are acted upon by the HR components (65, 66). Studies in bacteria have shown that inactivated replication forks can restart the process by reassembly of the replication machinery by different pathways, suggesting the possible occurrence of different structures at stalled forks (3, 9). The observation that a similar integration of replication and recombination exists in eukaryotes points out that this connection may be a widespread phenomenon (51, 55, 72–75).

Although genetic studies have demonstrated a critical role for *E. coli* RuvAB in RFR, the mechanism has not been clearly defined. *E. coli* RuvAB, a quintessential paradigm of HJ-binding

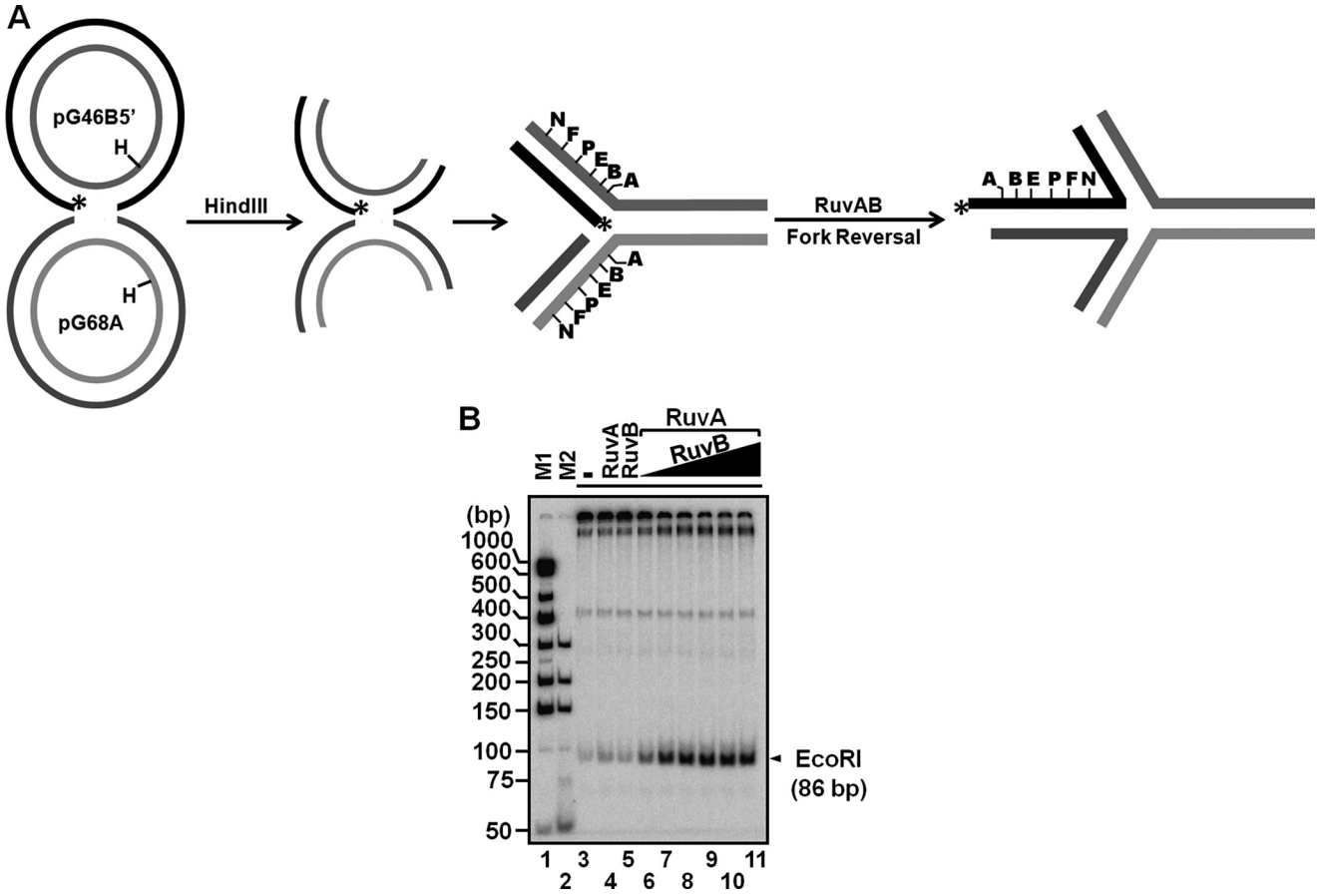

FIGURE 8. **MtRuvAB-mediated fork reversal is uncoupled from DNA supercoiling.** *A,* schematic diagram of the DNA substrate (RF digested with HindIII) and the outcome of RuvAB-mediated fork reversal reaction. Restriction endonuclease cleavage sites are indicated by the following letters: *A,* AvrII; *B,* BamHI; *E,* EcoRI; *P,* PvuII; F, AflIII, and *N,* AlwnI. *Asterisk* indicates the ^{32}P-labeled 5′-end of lagging daughter strand. *B,* RuvAB-mediated fork reversal of RF/HindIII-digested substrate, as monitored by digestion with EcoRI. *Lane 1* (*M1*), ^{32}P-labeled Gene Ruler 50-bp DNA ladder; *lane 2* (*M2*), ^{32}P-labeled Gene Ruler ultra low range DNA ladder; *lane 3*, 1 nM ^{32}P-labeled substrate in the absence of RuvAB; *lane 4,* 1 nM ^{32}P-labeled substrate in the presence of 1000 nM MtRuvA; *lane 5,* 1 nM ^{32}P-labeled substrate in the presence of 200 nM MtRuvB. *Lanes 6–11,* 1 nM ^{32}P-labeled substrate in the presence of 1000 nM MtRuvA and 100, 200, 300, 400, 500, 750, and 1000 nM MtRuvB, respectively. The *filled triangle* at the *top* of the gel image denotes increasing concentrations of MtRuvB.

and branch migration motor, is nearly ubiquitous in prokaryotes (67). In addition, genetic studies implicate this enzyme complex in RFR (15, 37, 38). However, it remains to be established if processing of stalled forks via RFR is universal across all prokaryotes. In *E. coli*, in addition to RuvAB, RecG plays a crucial role in the unwinding of a variety of branched DNA structures, including D-loops, R-loops, and stalled replication forks to create an HJ, albeit through distinct pathways (43).

Previously, it was demonstrated that *E. coli* RuvAB has the capacity to promote unwinding of replication forks primarily in the direction opposite that needed for HJ formation (47). Based on these findings, it was surmised that RuvAB may not be able to catalyze the formation of HJs from stalled replication forks. Furthermore, it has been suggested that RecG is likely to create HJs from stalled replication forks, whereas RuvAB acts predominantly at preexisting HJs (41, 48). However, the lack of genetic evidence for the role of RecG in both RFR and processing of stalled forks with a lesion on the leading strand does not correlate with the *in vitro* evidence, implicating the role of RecG in fork processing (15). In contrast, genetic data suggest a role for RuvAB-catalyzed RFR in certain replication mutants (15). This observation has been further supported by the isolation of *ruvA ruvB* mutants that are specifically impaired for fork reversal but not for HJ processing (37, 38). Taken together, these findings provided a rationale for examining the role of RuvAB in the processing of stalled replication forks.

To this end, we analyzed the RFR using *M. tuberculosis* RuvAB complex. The ability of *M. tuberculosis ruvA* and *M. tuberculosis ruvB* to rescue the UV and MMS sensitivity of *E. coli* Δ*ruvA* (26) and *E. coli* Δ*ruvB* cells (this study), respectively, suggest their physical interaction with RuvC of the resolvasome. Previous work has shown that RuvAB-HJ complexes were detected by EMSA in the presence of ATPγS, and the products were fixed by treatment with glutaraldehyde prior to electrophoresis (22). Like *E. coli* RuvB, our data show that MtRuvB lacks the capacity for stable binding to different DNA substrates. The data presented in Fig. 1*K* suggests a strong correlation between the extent of cooperative binding of MtRuvB and the nature of branched DNA structures. These results are consistent with the notion that the cooperative binding of RuvB is a combination of protein-protein interactions among RuvB monomers and between RuvA and RuvB. However, a key distinction in the observed differences in the extent of unwinding between homologous and heterologous HJs may arise from cooperativity between RuvA and RuvB and differences in the global alteration as well as unwinding modes of these struc-

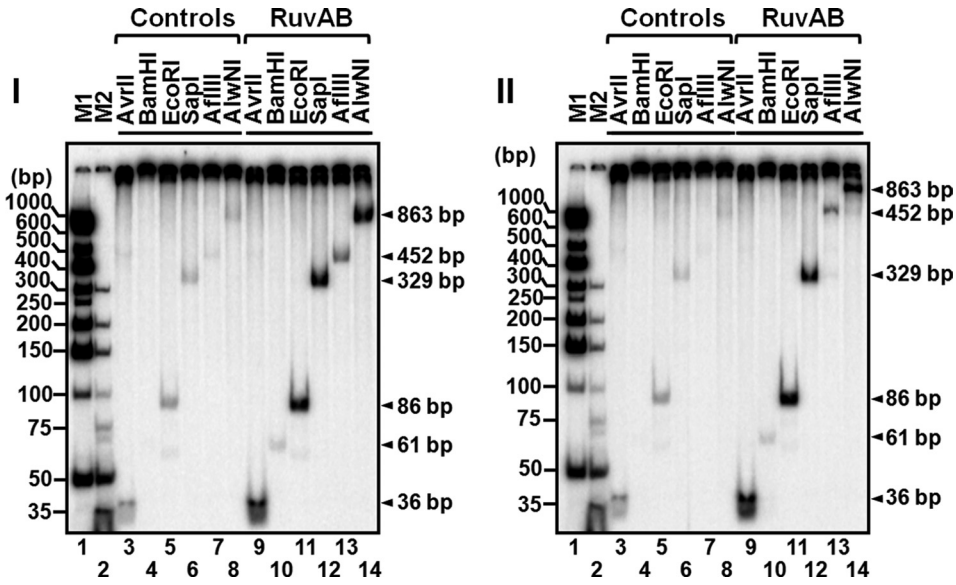

FIGURE 9. **MtRuvAB-catalyzed RFR is not impeded by the presence of a short heterologous sequence.** *I,* MtRuvAB-catalyzed RFR reaction with homologous JM. *II,* MtRuvAB-catalyzed RFR reaction with the JM-bearing heterologous insert. The assay was performed with the indicated ^{32}P-labeled substrate (1 nM), ATP (2 mM) in the absence or presence of a fixed amount of MtRuvA (1000 nM), and MtRuvB (200 nM). The formation of reversed arm was monitored by digestion using restriction enzymes. The different restriction enzymes used are indicated at the *top* of each lane, and the size of different products generated by restriction endonucleases is shown on the *right side* of gel image. *Lane 1, M1,* ^{32}P-labeled Gene Ruler 50-bp DNA ladder; *lane 2, M2,* ^{32}P-labeled Gene Ruler ultra low range DNA ladder. *Lanes 3–8* in both the panels show the DNA fragments generated in the absence of RuvAB. *Lanes 9–14* in both the panels depict the DNA fragments generated in the presence of RuvAB.

tures. Consistent with this, here we show that MtRuvAB exhibits the RFR activity on model substrates. Furthermore, these reactions showed enzyme concentration- and time-dependent conversion of substrate(s) into parental and daughter duplexes, the *bona fide* products of fork reversal under *in vitro* conditions. Specifically, the formation of daughter duplex is indicative of fork reversal as it encompasses the coordinated unwinding and pairing of the physically separated neo-daughter stands. Notably, our observations also show that the formation of leading or lagging daughter strand DNA is negligible, and catalytic concentration of MtRuvAB complex does not promote annealing of free daughter strand DNA, thus indicating that unwinding and annealing of daughter strands are kinetically indistinguishable. The formation of parental-daughter partial duplex is negligible, demonstrating that neither the primary nor secondary unwinding reactions favor their formation. Kinetics for the appearance of daughter as well as parental duplex were independent of the disposition of daughter strands at the fork junction. Our observations of RFR with an ensemble of fork substrates points out that the efficiency of *in vitro* fork reversal is independent of symmetry at the fork junction. These results support the idea that branch migration of the HJ intermediate results in the formation of parental and daughter duplex as the end product of the RFR reaction. Efficient reversal of plasmid-based model RF substrate by MtRuvAB strongly supports a conserved role for RuvAB complex in chromosome dynamics during fork stalling resulting from inactivation of replisome components. Analysis of fork reversal using RF substrates carrying hemi-replicated DNA corroborated our observation with synthetic homologous fork substrates that symmetry at the fork junction is dispensable for RuvAB complex-catalyzed fork reversal. Moreover, bypass of heterologous regions during MtRuvAB-catalyzed extensive fork reversal might have implications for genome stability and maintenance.

An important question arises from the findings described above. How are the forks substrates bearing different structures at the junction efficiently processed by the RuvAB complex? At first instance it might appear that single-stranded regions at the fork junction might interfere with processing of the fork substrates by RuvAB. Results from DNA binding assays in this study and some previous studies suggest that RuvA binds with high affinity to single strand DNA regions over duplex DNA (68). Thus, homologous fork substrates with the single-stranded region on either leading or lagging daughter strands would still support high affinity binding of RuvA at the fork junction. Consequently, formation of stable RuvAB-fork complex will result in similar efficiency of reversal observed with different homologous fork substrates having asymmetric fork junction.

The binding of RuvA to HJ intermediates initiates the assembly of hexameric RuvB rings through specific protein-protein interaction between domain III of RuvA and β-hairpin of N-terminal domain of RuvB (32). Crystallographic data further suggest that in an octameric RuvA-RuvB-HJ complex, the domain III looping out from adjacent subunits of tetrameric RuvA is not equivalent, and only two of four domain IIIs actually interact with RuvB monomer(s) (32). During the processing of the Y-junction by RuvAB, asymmetric binding of the RuvA tetramer at the junction directs the assembly of the single hexameric ring of RuvB on the parental duplex arm, and the resultant complex catalyzes unidirectional branch migration of these junctions (50). Moreover, the processing of Y-junctions by the RuvA mutant, incapable of forming an octameric complex, indicates that a tetramer of RuvA bound at the Y-junction can

guide the assembly of a single hexameric RuvB ring onto one of the arms (69). Recent results suggest that the formation of the RuvA octamer is essential for RuvAB-catalyzed replication fork reversal *in vivo* (33). Accordingly, during the processing of fork substrates by RuvAB, an assembly can be envisaged wherein octameric RuvA would guide the assembly of a single hexameric RuvB ring on the template strand of the fork. The acidic pins of RuvA might help in disruption of base pairs of the parental-daughter arms. Subsequently, motor activity of the RuvB ring would lead to the extrusion of the fourth arm at the fork junction thus generating an HJ intermediate. Once the HJ intermediate has been generated, assembly of a second RuvB ring, onto the extruded arm of the fork, will result in establishment of functional RuvAB-HJ branch migration complex. Thus, a likely scenario explaining the inability of *E. coli* RuvAB to convert replications forks into an HJ may be due to the nature of the substrates or *in vitro* experimental conditions.

Although RuvA and RuvB are among the well conserved protein components of the prokaryotic HR pathway, the eukaryotic genomes lack the structural homologs of *E. coli* RuvAB proteins. However, different lines of evidence suggest a role for RFR in phages, *S. cerevisiae,* and mammalian cells (2, 3). The components that have been shown to regulate replication stress response and fork regression include UvsW (70), Rad5 (59), RecQ5β (71), WRN (51, 72, 76), BLM (55, 72), FANCM and Fml1 (73, 74), and HLTF (77, 78). The mechanism of action of DNA helicases with respect to different replication fork substrates varies. However, of particular interest are WRN, BLM, and FANCM, which are implicated in human genetic diseases, characterized by premature aging syndromes, and cancer predisposition, respectively. Although RFR and the biological role of these proteins have not been demonstrated *in vivo*, it is possible that fork regression might have a crucial function in genome stability. Indeed, a crucial function of fork regression *in vivo* might be to avoid the formation of overt DNA breaks that contribute to genome instability, and our findings provide insights into the process of replication fork reversal catalyzed by RuvAB proteins. In light of the up-regulation of the *ruvA ruvB* expression during infection, an understanding of the MtRuvAB RFR activity will increase our knowledge of MtRuvAB and can lead to the processes of drug discovery and development.

Acknowledgments—We thank Dr. Leonard Wu for providing plasmids pG68 and pG46 and Dr. Hideo Shinagawa for providing the E. coli HRS3401 (ruvB::Km^R) strain.

REFERENCES

1. Kuzminov, A. (1999) *Microbiol. Mol. Biol. Rev.* **63,** 751–813
2. Michel, B. (2000) *Trends Biochem. Sci.* **25,** 173–178
3. Atkinson, J., and McGlynn, P. (2009) *Nucleic Acids Res.* **37,** 3475–3492
4. Cox, M. M., Goodman, M. F., Kreuzer, K. N., Sherratt, D. J., Sandler, S. J., and Marians, K. J. (2000) *Nature* **404,** 37–41
5. Carr, A. M. (2002) *Science* **297,** 557–558
6. Nohmi, T. (2006) *Annu. Rev. Microbiol.* **60,** 231–253
7. Michel, B., Flores, M. J., Viguera, E., Grompone, G., Seigneur, M., and Bidnenko, V. (2001) *Proc. Natl. Acad. Sci. U.S.A.* **98,** 8181–8188
8. Michel, B., Grompone, G., Florès, M. J., and Bidnenko, V. (2004) *Proc. Natl. Acad. Sci. U.S.A.* **101,** 12783–12788
9. Michel, B., Boubakri, H., Baharoglu, Z., LeMasson, M., and Lestini, R. (2007) *DNA Repair* **6,** 967–980
10. McGlynn, P., and Lloyd, R. G. (2002) *Nat. Rev. Mol. Cell Biol.* **3,** 859–870
11. Marians, K. J. (2000) *Trends Biochem. Sci.* **25,** 185–189
12. Grompone, G., Ehrlich, D., and Michel, B. (2004) *EMBO Rep.* **5,** 607–612
13. Heller, R. C., and Marians, K. J. (2006) *Nature* **439,** 557–562
14. Xu, L., and Marians, K. J. (2003) *Mol. Cell* **11,** 817–826
15. Baharoglu, Z., Petranovic, M., Flores, M. J., and Michel, B. (2006) *EMBO J.* **25,** 596–604
16. Seigneur, M., Ehrlich, S. D., and Michel, B. (2000) *Mol. Microbiol.* **38,** 565–574
17. Seigneur, M., Bidnenko, V., Ehrlich, S. D., and Michel, B. (1998) *Cell* **95,** 419–430
18. Cox, M. M. (2002) *Mutat. Res.* **510,** 107–120
19. Iwasaki, H., Takahagi, M., Shiba, T., Nakata, A., and Shinagawa, H. (1991) *EMBO J.* **10,** 4381–4389
20. Iwasaki, H., Takahagi, M., Nakata, A., and Shinagawa, H. (1992) *Genes Dev.* **6,** 2214–2220
21. Müller, B., Tsaneva, I. R., and West, S. C. (1993) *J. Biol. Chem.* **268,** 17179–17184
22. Parsons, C. A., and West, S. C. (1993) *J. Mol. Biol.* **232,** 397–405
23. Parsons, C. A., Stasiak, A., Bennett, R. J., and West, S. C. (1995) *Nature* **374,** 375–378
24. Parsons, C. A., Stasiak, A., and West, S. C. (1995) *EMBO J.* **14,** 5736–5744
25. Ariyoshi, M., Nishino, T., Iwasaki, H., Shinagawa, H., and Morikawa, K. (2000) *Proc. Natl. Acad. Sci. U.S.A.* **97,** 8257–8262
26. Khanduja, J. S., Tripathi, P., and Muniyappa, K. (2009) *Biochemistry* **48,** 27–40
27. Hargreaves, D., Rice, D. W., Sedelnikova, S. E., Artymiuk, P. J., Lloyd, R. G., and Rafferty, J. B. (1998) *Nat. Struct. Biol.* **5,** 441–446
28. Chamberlain, D., Keeley, A., Aslam, M., Arenas-Licea, J., Brown, T., Tsaneva, I. R., and Perkins, S. J. (1998) *J. Mol. Biol.* **284,** 385–400
29. Rafferty, J. B., Ingleston, S. M., Hargreaves, D., Artymiuk, P. J., Sharples, G. J., Lloyd, R. G., and Rice, D. W. (1998) *J. Mol. Biol.* **278,** 105–116
30. Roe, S. M., Barlow, T., Brown, T., Oram, M., Keeley, A., Tsaneva, I. R., and Pearl, L. H. (1998) *Mol. Cell* **2,** 361–372
31. Tsaneva, I. R., Illing, G., Lloyd, R. G., and West, S. C. (1992) *Mol. Gen. Genet.* **235,** 1–10
32. Yamada, K., Miyata, T., Tsuchiya, D., Oyama, T., Fujiwara, Y., Ohnishi, T., Iwasaki, H., Shinagawa, H., Ariyoshi, M., Mayanagi, K., and Morikawa, K. (2002) *Mol. Cell* **10,** 671–681
33. Bradley, A. S., Baharoglu, Z., Niewiarowski, A., Michel, B., and Tsaneva, I. R. (2011) *J. Biol. Chem.* **286,** 22372–22383
34. Tsaneva, I. R., Müller, B., and West, S. C. (1992) *Cell* **69,** 1171–1180
35. Prabu, J. R., Thamotharan, S., Khanduja, J. S., Chandra, N. R., Muniyappa, K., and Vijayan, M. (2009) *Biochim. Biophys. Acta* **1794,** 1001–1009
36. West, S. C. (1997) *Annu. Rev. Genet.* **31,** 213–244
37. Baharoglu, Z., Bradley, A. S., Le Masson, M., Tsaneva, I., and Michel, B. (2008) *PLoS Genet.* **4,** e1000012
38. Le Masson, M., Baharoglu, Z., and Michel, B. (2008) *Mol. Microbiol.* **70,** 537–548
39. McGlynn, P., and Lloyd, R. G. (2000) *Cell* **101,** 35–45
40. McGlynn, P., and Lloyd, R. G. (2001) *Proc. Natl. Acad. Sci. U.S.A.* **98,** 8227–8234
41. McGlynn, P., Lloyd, R. G., and Marians, K. J. (2001) *Proc. Natl. Acad. Sci. U.S.A.* **98,** 8235–8240
42. Donaldson, J. R., Courcelle, C. T., and Courcelle, J. (2004) *Genetics* **166,** 1631–1640
43. Rudolph, C. J., Upton, A. L., Briggs, G. S., and Lloyd, R. G. (2010) *DNA Repair* **9,** 210–223
44. Rachman, H., Strong, M., Ulrichs, T., Grode, L., Schuchhardt, J., Mollenkopf, H., Kosmiadi, G. A., Eisenberg, D., and Kaufmann, S. H. (2006) *Infect. Immun.* **74,** 1233–1242
45. Dresser, A. R., Hardy, P. O., and Chaconas, G. (2009) *PLoS Pathog.* **5,** e1000680
46. Lin, T., Gao, L., Edmondson, D. G., Jacobs, M. B., Philipp, M. T., and Norris, S. J. (2009) *PLoS Pathog.* **5,** e1000679
47. McGlynn, P., and Lloyd, R. G. (2001) *J. Biol. Chem.* **276,** 41938–41944

48. Thomason, L. C., Costantino, N., and Court, D. L. (2007) *Curr. Protoc. Mol. Biol.* **79,** 1.17.1–1.17.8
49. Hiom, K., and West, S. C. (1995) *Cell* **80,** 787–793
50. Hiom, K., Tsaneva, I. R., and West, S. C. (1996) *Genes Cells* **1,** 443–451
51. Machwe, A., Xiao, L., Lloyd, R. G., Bolt, E., and Orren, D. K. (2007) *Nucleic Acids Res.* **35,** 5729–5747
52. Svoboda, D. L., and Vos, J. M. (1995) *Proc. Natl. Acad. Sci. U.S.A.* **92,** 11975–11979
53. Pagès, V., and Fuchs, R. P. (2003) *Science* **300,** 1300–1303
54. Flores, M. J., Bierne, H., Ehrlich, S. D., and Michel, B. (2001) *EMBO J.* **20,** 619–629
55. Ralf, C., Hickson, I. D., and Wu, L. (2006) *J. Biol. Chem.* **281,** 22839–22846
56. Higgins, N. P., Kato, K., and Strauss, B. (1976) *J. Mol. Biol.* **101,** 417–425
57. Postow, L., Ullsperger, C., Keller, R. W., Bustamante, C., Vologodskii, A. V., and Cozzarelli, N. R. (2001) *J. Biol. Chem.* **276,** 2790–2796
58. Dennis, C., Fedorov, A., Käs, E., Salomé, L., and Grigoriev, M. (2004) *EMBO J.* **23,** 2413–2422
59. Blastyák, A., Pintér, L., Unk, I., Prakash, L., Prakash, S., and Haracska, L. (2007) *Mol. Cell* **28,** 167–175
60. Hanawalt, P. C. (1966) *Photochem. Photobiol.* **5,** 1–12
61. Skalka, A. (1974) in *Mechanisms in Recombination* (Grell, R. F., ed) pp. 421–432, Plenum Publishing Corp., New York
62. Otsuji, N., Iyehara, H., and Hideshima, Y. (1974) *J. Bacteriol.* **117,** 337–344
63. Shurvinton, C. E., Lloyd, R. G., Benson, F. E., and Attfield, P. V. (1984) *Mol. Gen. Genet.* **194,** 322–329
64. Ishioka, K., Fukuoh, A., Iwasaki, H., Nakata, A., and Shinagawa, H. (1998) *Genes Cells* **3,** 209–220
65. Lusetti, S. L., and Cox, M. M. (2002) *Annu. Rev. Biochem.* **71,** 71–100
66. Sogo, J. M., Lopes, M., and Foiani, M. (2002) *Science* **297,** 599–602
67. Rocha, E. P., Cornet, E., and Michel, B. (2005) *PLoS Genet.* **1,** e15
68. Shiba, T., Iwasaki, H., Nakata, A., and Shinagawa, H. (1991) *Proc. Natl. Acad. Sci. U.S.A.* **88,** 8445–8449
69. Privezentzev, C. V., Keeley, A., Sigala, B., and Tsaneva, I. R. (2005) *J. Biol. Chem.* **280,** 3365–3375
70. Long, D. T., and Kreuzer, K. N. (2009) *EMBO Rep.* **10,** 394–399
71. Kanagaraj, R., Saydam, N., Garcia, P. L., Zheng, L., and Janscak, P. (2006) *Nucleic Acids Res.* **34,** 5217–5231
72. Machwe, A., Xiao, L., Groden, J., and Orren, D. K. (2006) *Biochemistry* **45,** 13939–13946
73. Gari, K., Décaillet, C., Delannoy, M., Wu, L., and Constantinou, A. (2008) *Proc. Natl. Acad. Sci. U.S.A.* **105,** 16107–16112
74. Sun, W., Nandi, S., Osman, F., Ahn, J. S., Jakovleska, J., Lorenz, A., and Whitby, M. C. (2008) *Mol. Cell* **32,** 118–128
75. Bugreev, D. V., Rossi, M. J., and Mazin, A. V. (2011) *Nucleic Acids Res.* **39,** 2153–2164
76. Machwe, A., Lozada, E., Wold, M. S., Li, G. M., and Orren, D. K. (2011) *J. Biol. Chem.* **286,** 3497–3508
77. Blastyák, A., Hajdú, I., Unk, I., and Haracska, L. (2010) *Mol. Cell. Biol.* **30,** 684–693
78. Achar, Y. J., Balogh, D., and Haracska, L. (2011) *Proc. Natl. Acad. Sci. U.S.A.* **108,** 14073–14078